



# Steel plate shear walls with large disconnected lengths of web plate to vertical boundary element

Mohammad Reza Hajimirsadeghi, Nader Fanaie \*

Department of Civil Engineering, K. N. Toosi University of Technology, Tehran, Iran

## ARTICLE INFO

### Keywords:

Steel plate shear wall  
Partial length connection  
Analytical solution  
Vertical Boundary Element (VBE)  
Finite element method

## ABSTRACT

Steel plate shear walls as lateral load resisting systems provide resistance to seismic and wind forces in buildings. The partial length connection web plate to vertical boundary element steel plate shear walls, which lacks the connection at the middle height of VBE has been recently introduced by researchers. This novel steel shear wall was proposed as a key approach so as to reduce column's significant demand due to resistance of web plate diagonal yielding in conventional steel plate shear walls. In this survey the design of the proposed shear walls with regard to large value of not connected length ratio of web plate to vertical boundary element was considered. Development of the tension field action across the entire width of the proposed shear walls considering different panel aspect ratios and various number of stories were investigated by establishing 27 numerical models (3 groups of 9 groups) using finite element Abaqus software. The available experimental data was used to validate the modeling methodology. The pushover analyses were performed for all the models. Finally, based on the presented numerical investigation, the equations governing the system, including panel shear strength and the angle of inclination of the tensile field, which are valid for not connection length ratio larger than thirty percent, were analytically developed.

## 1. Introduction

Steel plate shear walls (SPSW) have been utilized in buildings over the world since early 1970s [1]. Experimental and numerical researches on SPSW have revealed their ability to behave in a ductile manner as well as their capability of dissipating significant amounts of energy when subjected to cyclic inelastic loadings [2–8]. To achieve a ductile global response from a steel plate shear wall, a significant yielding needs to occur in web plate. The web yielding occurs due to the development of a diagonal tension field, and buckling of the plate in the orthogonal direction. The capacity design of Vertical Boundary Element (VBE) with regard to the resistance of the web plate expected yield strength in this diagonal direction could lead to substantial increase in column size [9–10]. This key problem leads to a lack of wide spread implementation of steel shear walls [9]. To address VBE significant demand due to the diagonal yielding in web plate, several techniques have been proposed by researchers, e.g., using low yield point steels and pure aluminum for the infill panels

[11–13], reduced-beam section connections to reduce HBE size

without any concern about in-span plastic hinge formation as main objective and as a byproduct reduction in HBE size due to decreasing frame action demand, strategic placement of holes in the infill panels [14], installation of pin-ended horizontal strut at mid-height of the VBE in a SPSW [15], separating the VBE (secondary column) from the original frame column (primary column) [16], using outrigger beams [17,18], coupling beams [19], and irregular wall configurations such as staggered arrangement of web plate [20] to reduce overturning forces on VBE in high-rise buildings. As interest in this research, some of them have tackled this problem by reconsidering the attachment of web plates to a vertical boundary element [21–31] in two ways. The first approach, i.e. the older one, was to exempt column from contribution in web plate anchoring role and assign this role to beam elements. As a result, the boundary columns were not subjected to the lateral forces due to tension field development in the web plate. This approach was proposed for the first time by Xue and Lu [21] by conducting numerical research, and followed by Choi and Park [22], Guo et al. [23], and Vatansever and Yardimci [24] by performing experimental studies. It was studied comprehensively by Qian and Astane-asl [25] as well. Those studies

\* Corresponding author at: K. N. Toosi University of Technology, Civil Engineering Department, No. 1346, Vali-Asr Street, P.O. Box. 15875-4416, 19697 Tehran, Iran.

E-mail address: [fanaie@kntu.ac.ir](mailto:fanaie@kntu.ac.ir) (N. Fanaie).

<https://doi.org/10.1016/j.istruc.2021.10.056>

Received 30 July 2021; Received in revised form 3 October 2021; Accepted 17 October 2021

2352-0124/© 2021 Institution of Structural Engineers. Published by Elsevier Ltd. All rights reserved.

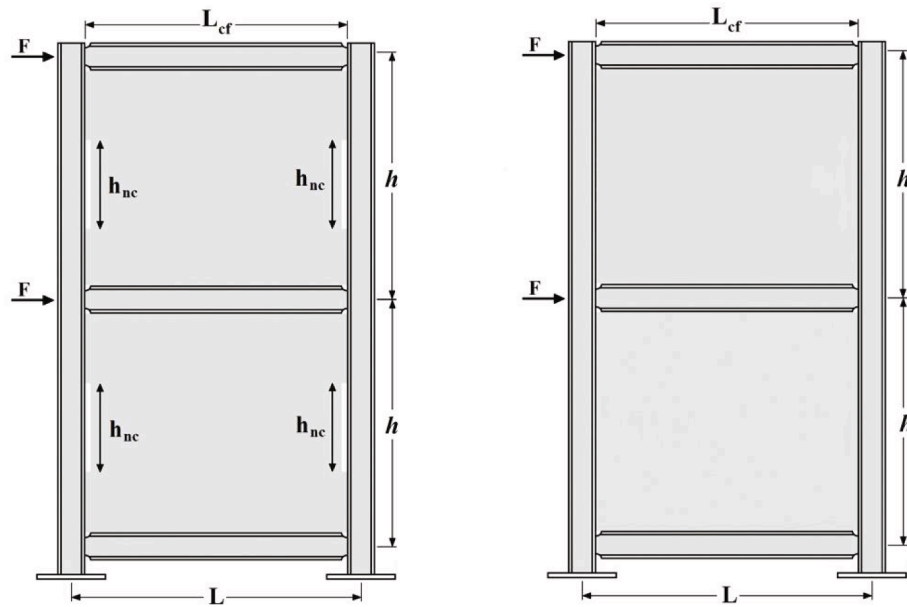


Fig. 1. Steel plate shear wall with partial length connection of infill plate to VBE in comparison with the conventional steel plate shear wall; (a) partial length connection steel plate shear wall; (b) conventional steel plate shear wall.

Table 1

The considerations in modeling methodology regarding the three laboratory tests.

Laboratory test	Panel aspect ratio ( $L/h$ )	Story number	Description
Li et al. [32]	0.9	2	Two-story small aspect ratio specimen
Vian et al. [33,34]	2	1	Single-story average aspect ratio specimen
Choi and Park [35]	2.05	3	Three-story large aspect ratio specimen

demonstrated that detaching web plate from connecting to VBE had admissible merit in reducing the flexural demands on the columns of the boundary frame, and permitting to adjust load-carrying capacity and initial stiffness of shear wall by changing web plate thickness without being concerned about the flexural demand of the column. Hence, SPSW with infill plates attached only to the beams would be useful in retrofitting and strengthening the steel frames which have inadequate stiffness and strength [24]. However, this kind of steel shear walls has some disadvantages such as losing VBE ability in mobilizing web plate shear strength and degrading the panel ductile behavior owing to the web plate out of plane displacement at the vertical free edges adjacent to VBE. The last item caused researcher to attach thick stiffener in this area to eliminate out of plane deformation [22,25]. The Second approach introduced by [26,31] using partial length connection between web plate and VBE, which lacks the connection at the middle of the height of VBE to compromise between merits and demerits. Fig. 1 illustrates the idea of partial connection of web plate to VBE in a two-story steel shear wall with pin connections of the boundary elements to each other and VBE to the base, in comparison with the conventional steel plate shear wall. In Fig. 1,  $h_{nc}$  (nc = not connected) presents the length of the central part of the infill plate, which was not connected to VBE;  $h$  denotes the distance between HBE centerlines,  $L$  presents the distance between VBE centerlines, and  $NCR$  stands for the not connected length ratio ( $NCR = h_{nc}/h$ ). It should be noted that in determining  $NCR$  in this figure, the beam height effect was neglected for simplicity.

As it could be implied, the purpose of this idea is to shift the heavy distributed loads created at mid span of VBE because of tension field

formation to be closer to the support to reduce VBE flexural and stiffness demands. This idea for the first time was implicitly introduced by Wei et al. [26–29] in which a quarter of the height/width of the restrained steel web plate (sandwiched between bilateral pre-cast RC panels [26–28]) was attached to the surrounding boundary elements whereas the mid-height/width was not connected to the boundary elements. The experimental results of the studies carried out by the mentioned researchers exhibit high initial stiffness, adequate ductility, excellent energy absorption capacity, and stable hysteresis loop. Paslar et al. [30] numerically investigated the effect of various types of partial interconnection between web plates and boundary frame elements. According to their research, systems with lack of connection at the middle height of VBE revealed desirable structural behavior. Furthermore, with connectivity ratio of 80% with this type of connection, similar structural performances were observed compared to the conventional system with the steel plate shear wall fully connected to the infill plates. Exhaustive analytical studies were conducted recently by Hajimirsadeghi and Fanaie [31] based on numerical and experimental studies on partial length connection web plate to VBE steel plate shear wall. They investigated experimentally and numerically the parallelism in tension field strip inclination across the entire web plate for a case in which the not connected length ratio for a single-story building with a fixed panel aspect ratio (ratio of the length of the panel to its height:  $L/h = 1.33$ ) was less than 30%. Based on the achieved evidence they propose system governing equation, including panel shear strength, the angle of inclination of the tension field, and minimum stiffness requirements in vertical boundary elements. In this study a supplementary numerical investigation was conducted to consider the effect of various not connected length ratio (larger than 30%), panel aspect ratios ( $L/h$ ), and the number of stories to study stress state in web plate. Based on the study, the proposed system, analytical method, and the governing equations were developed for a considered range of not connected length ratio ( $NCR \geq 0.3$ ). For this purpose, the finite element models were initially established and validated based on the three laboratory tests. The laboratory tests represented a variety of panel aspect ratios ( $L/h$ ) and the number of stories. Twenty seven FEM models were developed based on the verified models, and various not connected infill plate length ratios for each model were considered. The modeling was intended to investigate the quality of the formation of tension field across the entire width of the wall. Finally, based on the assumptions confirmed by

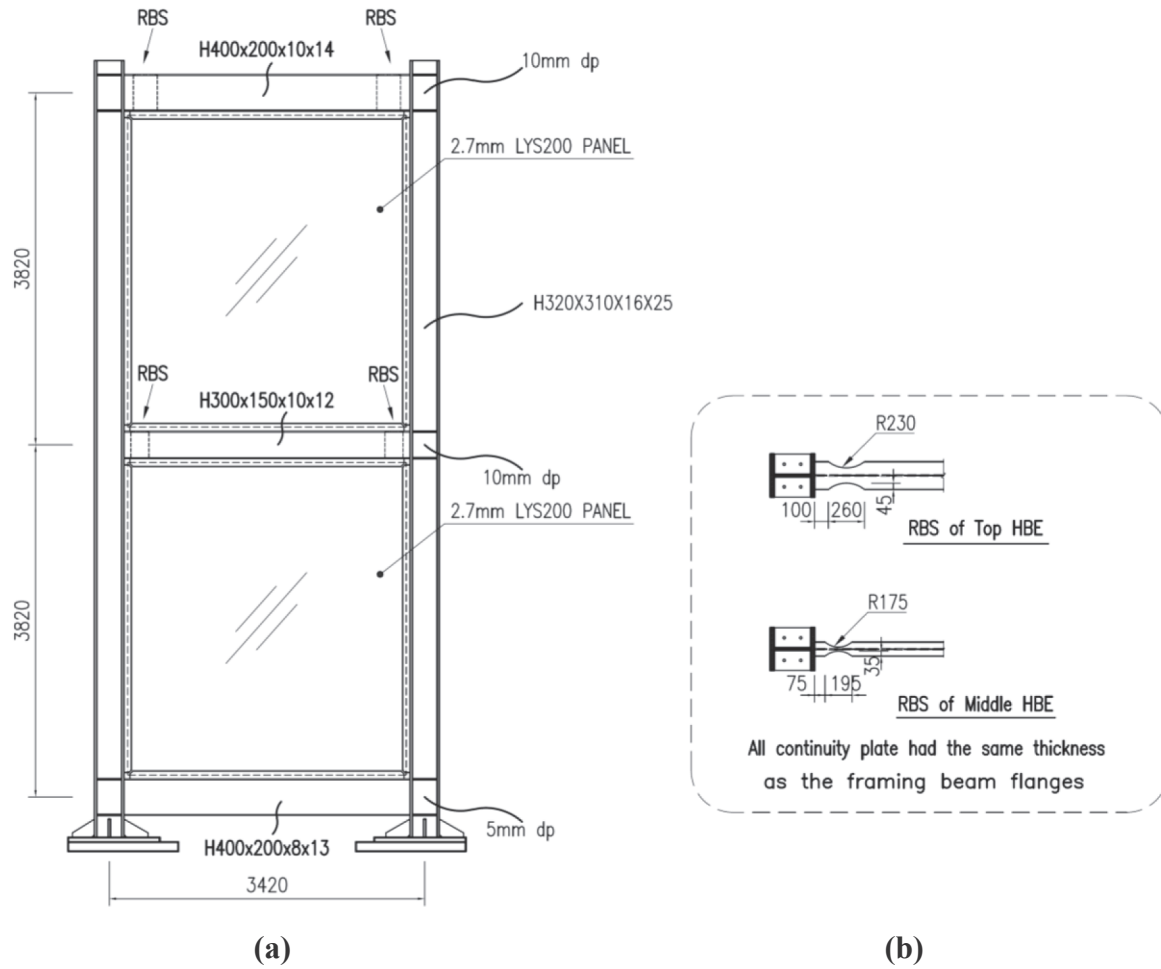


Fig. 2. The details of the normal column (NC) laboratory test specimen; (a) the overall dimensions; (b) the reduced beam section (RBS) details (Li et al. [32]).

Table 2  
Material properties [32].

Member	Section	Flange		Web	
		$F_y$ (MPa)	$F_u$ (MPa)	$F_y$ (MPa)	$F_u$ (MPa)
Top HBE	H400 × 200 × 10 × 14	405	537	464	561
Middle HBE	H300 × 150 × 10 × 12	372	506	464	561
Bottom HBE	H400 × 200 × 8 × 13	390	502	430	509
VBE	H320 × 310 × 16 × 25	386	547	389	564

aforementioned numerical modeling, the vertical boundary element governing equations were analytically developed.

## 2. Verification of the modeling methodology

To explain the quality of tension field formation in the presence of the infill plate without a connection in the middle height of the VBE, three dimensional numerical parametric studies were performed using the commercial finite element software, Abaqus 2016. The not connected length ratio of the infill plates was utilized as a variable in the parametric study. Three laboratory tests were considered to verify the methodology of the numerical modeling. The verification of the laboratory tests was performed based on the normal column (NC) specimen

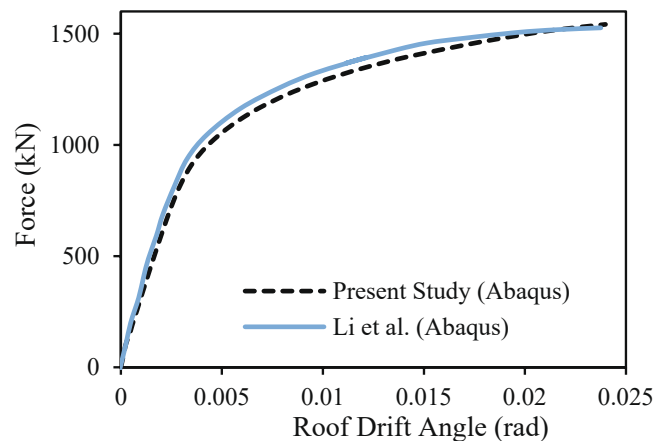


Fig. 3. Push-over results from the finite element modeling in this study and the study by Li et al.

by Li et al. [32], the S2 specimen by Vian et al. [33,34], and the FSPW 3 specimen by Choi et al. [35]. All of the above-mentioned studies were selected from previous experimental researches on the behavior of the steel plate shear walls. It should be noted that all of these three specimens experienced cyclic loadings. In these investigations the corresponding researchers used finite element modeling for push-over loading analysis, which was in accordance with experimental results.

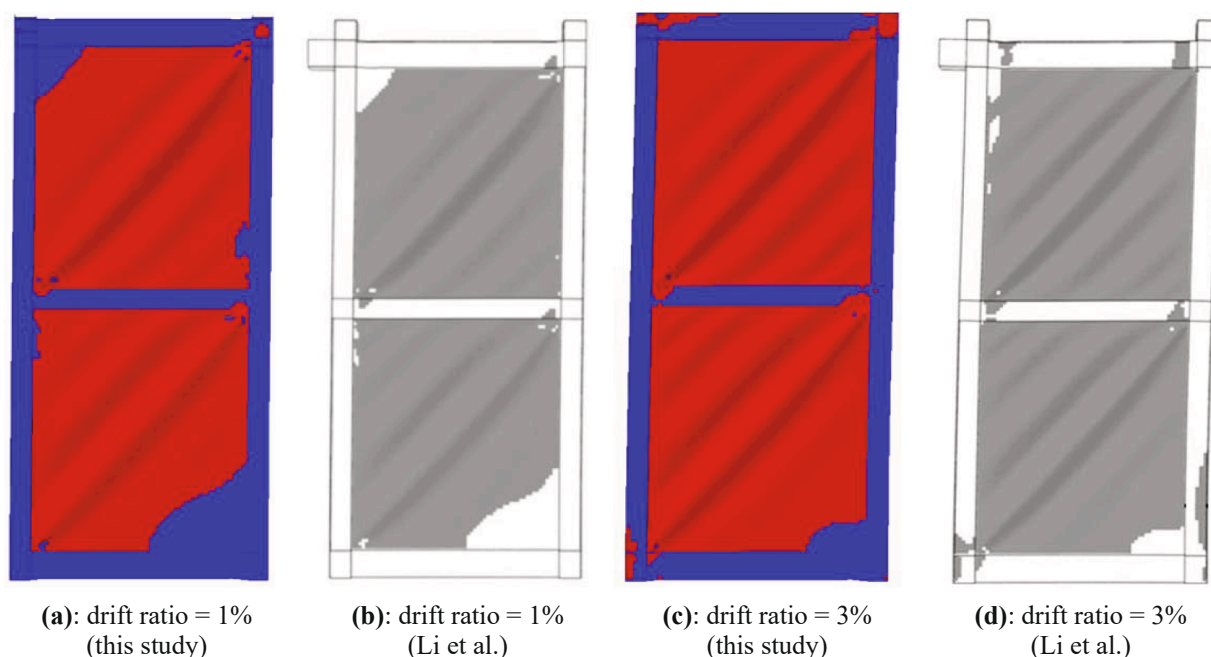


Fig. 4. The verification of the yielding zone from finite element modeling in this study with the results from Li et al.

Because of these study modelling requirements, verifications were carried out based on the results of the corresponding push-over modeling in the original research. The aspect ratio variation was selected based on the AISC341-05 [36] provisions for the design of SPSW, which limited their applicability to wall panels with aspect ratios of  $0.8 < L/h \leq 2.5$ . It should be mentioned that in recent AISC provision (341–16) [10] there is no limitation for the aspect ratio. Furthermore, this range of aspect ratio was used as a practical suggestion. These specimens were selected to represent the various situations of the panel aspect ratio, and the story number as presented in Table 1.

### 2.1. General considerations in the modeling

A typical steel plate shear wall panel generally consists of HBEs (edge beams), VBEs (edge columns), web plate, beam-to-column connections, and fish plates. The web and boundary elements for all considered cases were modeled by S4R shell elements, which are quadrilateral shell elements with 4 nodes (linear shape function) and reduced numbers of Gaussian integration points (1 point). The element has six degrees of freedom (3 translational and 3 rotational DOFs) at each node of the elements and considers both membrane and bending behavior. This kind of element is appropriate for both material and geometric nonlinearity [37]. Isotropic hardening rule (i.e., an expansion of the yield surface while undergoing plastic strains) is generally true for uniaxial stress state. Owing to the nearly uniaxial stress state experienced in the web plates and the boundary elements, due to the applied monotonic push-over loading, isotropic hardening rule was implemented. All mechanical properties were included in the finite element model. The web plates were welded at all edges to the surrounding boundary elements of all specimens. In modeling the specimens, the connection tab, or “fish plate”, which was utilized in the experiments to connect the web plate to the surrounding boundary elements was neglected in the finite element modeling. Instead, a direct connection was assumed to be between the two structural elements. Driver et al. [38] proved that a fish plate could be neglected in finite element model, and does not affect simulated results.

The initial shapes of the web plates used in three test specimens were not recorded prior to the tests. However, all webs were not ideally flat, but had insignificant out-of-plane deviations from perfect flatness. These

deviations occur due to various reasons such as improper transportation and installation, which are expected in construction. Those minor imperfections finally helped precipitate global panel buckling, and needed to be considered in the FE analysis. Eigenvalue buckling analyses were performed on the perfect structures (i.e. the undeformed models, prior to applying the push-over load) so as to account for the initial imperfections. Finally, the distributions of the imperfections were determined using the superposition of the selected buckling mode shapes. The buckling mode shapes were added to the perfect model using the imperfection command. The effect on the stiffness and strength of the SPSWs is very small and can be neglected as long as the magnitude of the initial imperfections is less than 1% of  $\sqrt{L_{cf}h}$ , where  $L_{cf}$  presents the length of the panel between column flanges, and  $h$  denotes the panel height [38].

The solution strategies for physical problems via nonlinear FEM are divided into two categories, namely implicit and explicit methods. The implicit method solution is employed for static and quasi-static analyses [37]. Therefore, due to the quasi-static type of SPSWs monotonic loading, for nonlinear analysis of FE models, an implicit method (quasi-static) was implemented. The implicit dynamic analysis was carried out in all simulations. Because of numerical instability and convergence problems due to buckling analysis, dynamic solver was used rather than static one, and the load was gradually applied so as to minimize the dynamic effect. To monitor the dynamic effect, ratio of kinetic energy to total energy was controlled in all analyses, and was observed to be negligible. There was a good consistency between the results of this study and those of the aforementioned researches, which confirms that the dynamic effect was insignificant. The Newton-Raphson method was used to solve the nonlinear equations of FE models. Further description regarding the details of the specimens utilized in the test, including the model geometry, the material properties, the mesh size, the loading protocol, and the imperfections applying techniques are explained below to ensure the reproducibility of the models.

### 2.2. The study by Li et al.

The first verified steel shear wall system was a single bay, two-story steel plate shear wall. The detailed dimensions of specimen are shown in Fig. 2. The four dimensions for H-shape sections, which are illustrated in

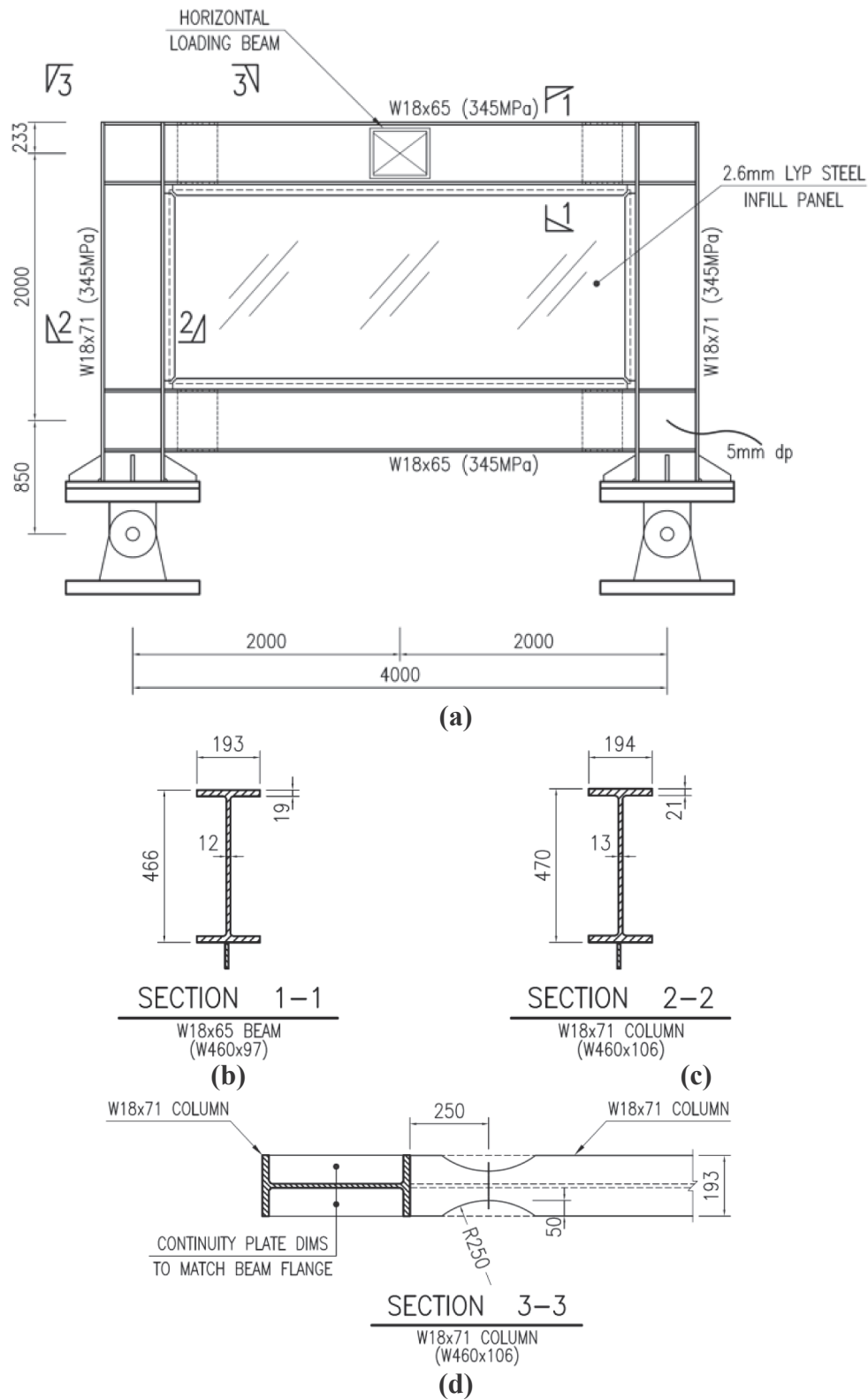


Fig. 5. Vian et al. S2 laboratory test specimen; (a) Overall dimensions, (b) Built-up W18x65 Beam Section, (c) Built-up W18x71 Column Section, (d) Reduced Beam Section detailing. [14,34].

Fig. 2 represent depth, flange width, web thicknesses, and flange thicknesses (in millimeter), respectively. The web plates were made of 2.7 mm thick steel with a low yield strength and with a measured yield stress of  $F_{yp} = 220$  MPa. The boundary elements and the stiffener plates used in the specimen were built-up sections, fabricated from plate

material specified as A572Gr50 steel [32].

Fig. 2(b) illustrates the details of the reduced beam section (RBS), which were adopted for the

HBE-to-VBE connections of TBs and MBs. The material properties were presented in Table 2.

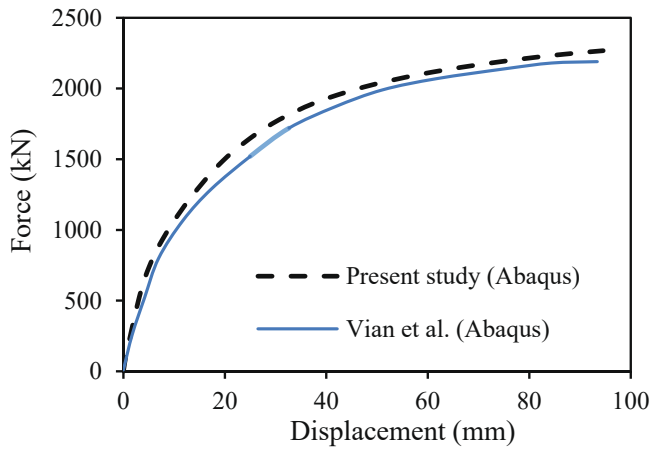


Fig. 6. Push-over results from finite element modeling in present study and Vian et al. study.

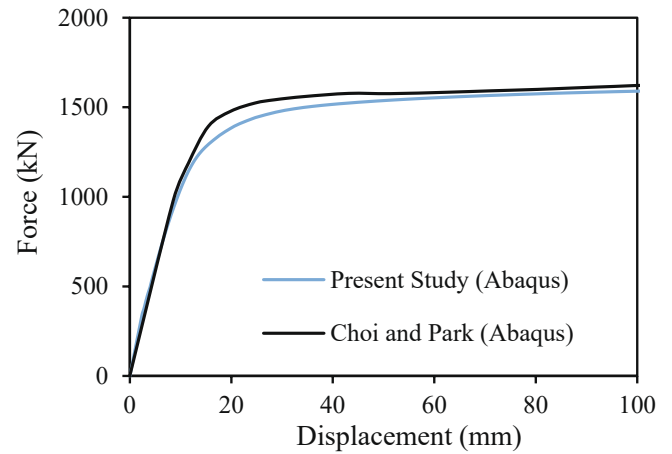


Fig. 8. Push-over results from finite element modeling in present study and Choi and Park.

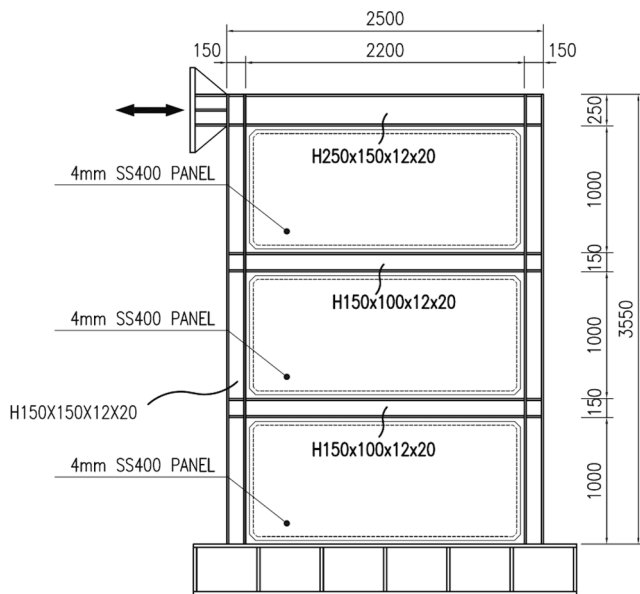


Fig. 7. FSPW3 laboratory test specimen (Choi and Park, [35]).

Table 3  
Material properties [35].

Grade	Thickness (mm)	$F_y$ (MPa)	$F_u$ (MPa)	Member
SS400	4	299	372	Infill panel
SM490	8	385	542	VBE (Web)
SM490	12	377	527	HBE (Web)
SM490	20	353	538	VBE-HBE (Flange)

A bilinear curve was considered to describe the stress–strain diagram of web plates and boundary elements. This bilinear stress–strain diagram extends from the origin to value of the coupon yield stresses. A post-yield stiffness of 0.01E (E is Young’s modulus) was considered after yield stresses. All mechanical properties were included in the finite element model. Both VBEs were clamped at their bases. In addition, the HBEs were prevented from any out-of-plane displacement. The initial distribution of the imperfection was determined using the superposition of the first two buckling mode shapes nodal displacement, multiplied by a small displacement amplitude of 2 mm using the Edit-Keywords in the Abaqus software.

A set of mesh sensitivity analyses were conducted, and a 50 × 50 mm

Table 4  
Numerical model codes according to the not connected length ratio.

Ref. Model	Not connected length ratio (NCR)	model codes
Li et al.	0%	L0
Vian et al.		V0
Choi and Park	10%	C0
Li et al.		L1
Vian et al.	V1	
Choi and Park	C1	
Li et al.	20%	L2
Vian et al.		V2
Choi and Park	C2	
Li et al.	30%	L3
Vian et al.		V3
Choi and Park	C3	
Li et al.	40%	L4
Vian et al.		V4
Choi and Park	C4	
Li et al.	50%	L5
Vian et al.		V5
Choi and Park	C5	
Li et al.	60%	L6
Vian et al.		V6
Choi and Park	C6	
Li et al.	80%	L8
Vian et al.		V8
Choi and Park	C8	
Li et al.	100%	L10
Vian et al.		V10
Choi and Park	C10	

refined mesh was selected for the shell elements following a trade-off between the computational cost and the desired accuracy in accordance with reference load–displacement results. Finally, the displacement controlled push-over loading was applied at the top beam in a left to right direction. Fig. 3 shows that the results of the load–displacement behavior from the finite element analysis in this study corresponds to the results of Li et al. [32] with a proper accuracy (Fig. 3). Fig. 4 compares yielding zone achieved from the modeling used in this study with the results from the modeling used by Li et al. in total drift ratio of 1% and 2%, respectively. As the figure shows, similar behavior was observed in both models.

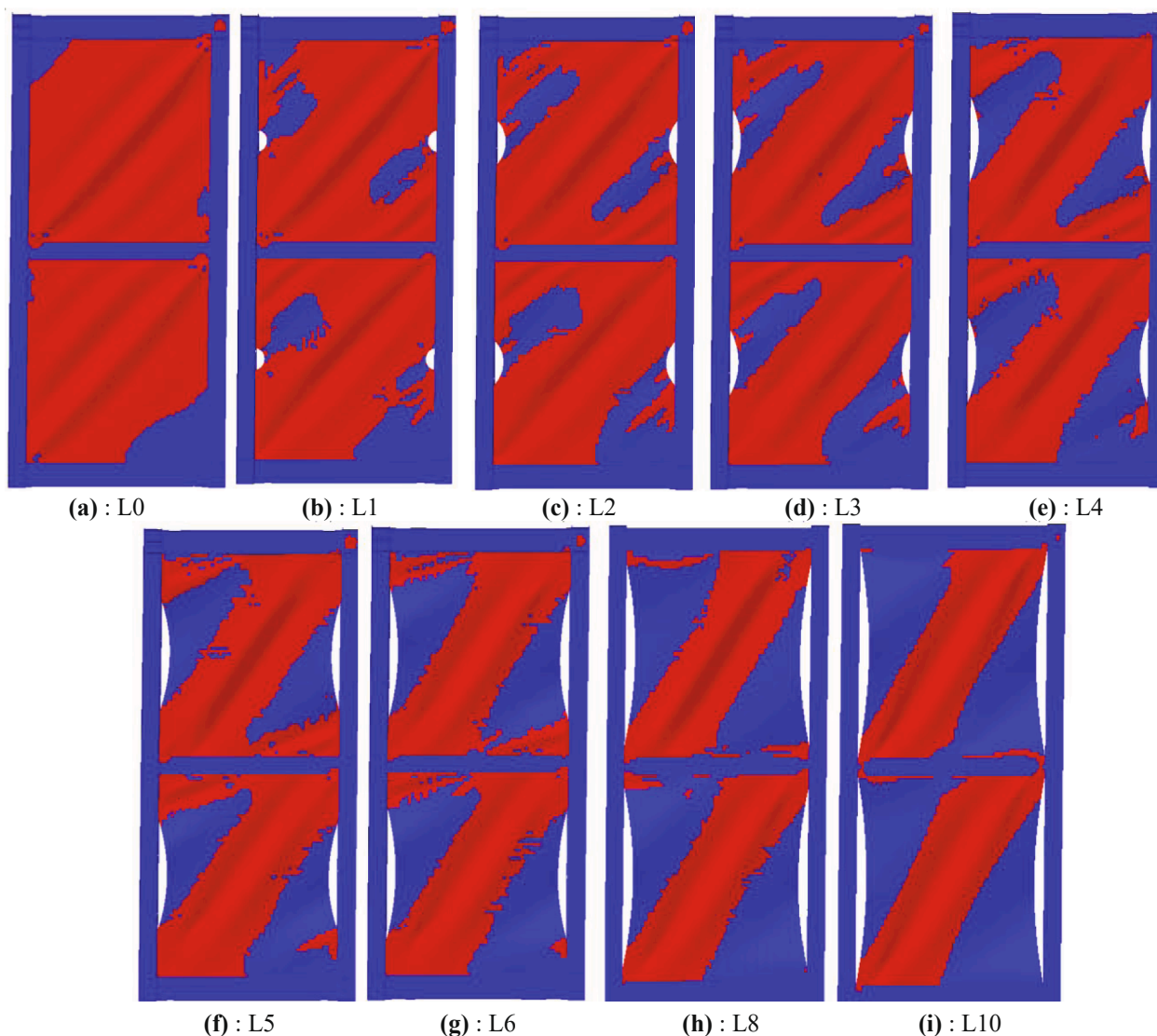


Fig. 9. The effect of the various not connected length ratios on the quality of the tension field formation in 1% total drift ratio.

### 2.3. The study by Vian et al.

The second verified steel shear wall system consists of a single-bay, single story frame, with reduced beam section type beam-to-column connections. The web plate was made of a 2.6 mm thick low yield strength steel LYS100 with a measured yield and ultimate stresses of 165 and 305 MPa, respectively resulted from the uniaxial tensile test. The web plate was welded at all edges to the surrounding boundary elements. The boundary frame members are made of ASTM A572 steel with the yield stress of 345 MPa and the ultimate stress of 448 MPa. The detailed dimensions of specimen are illustrated in Fig. 5. The hinge at the base of each column specimen was not explicitly modeled in the Abaqus software. Instead, the “CONN3D2” connector elements were employed to connect a reference node at the location of the hinge center to the nodes at the tip of each flange and the intersection of the flanges and web. All degrees of freedom, with the exception of rotation about the out-of-plane axis, were restrained at the reference node located at the center of the hinge to indicate the hinge rotation, which was allowed during the test. The out-of-plane resistance provided by the lateral supports at the top of the columns during the experiments was modeled by restraining displacements in that direction. The exterior nodes of the flange elements around the perimeter of the panel zones were restrained against movement in the z-direction.

The initial distribution of the imperfection was determined by the first buckling mode shape nodal displacements, multiplied by a small displacement amplitude of 1 mm using the Edit-Keywords in the Abaqus software. A set of mesh sensitivity analysis were conducted, and a  $50 \times 50$  mm refined mesh was selected for the shell elements following a trade-off between the computational cost and desired accuracy in accordance with reference load–displacement results. Finally, the displacement controlled push-over loading was applied at the middle of the top beam in a left to right direction. Fig. 6 shows a good accordance between the load–displacement behavior from the finite element modeling in this study and the results of Vian et al. [34], which confirms the proper accuracy of the modeling used in the current study.

### 2.4. The study by Choi and Park

The third verified steel shear wall system was a one-third model of a single-bay, three-story steel plate shear wall with fully restrained beam to column moment connections. The web plates were made of the 4-mm thick mild steel SS400 (Korean Standard) with a measured yield and the ultimate stresses of 299 and 372 MPa, respectively resulted from uniaxial tensile test. The detailed dimensions of specimen are presented in Fig. 7. The boundary elements and the stiffener plates used in the three specimens were fabricated from plate material specified as SM490 steel

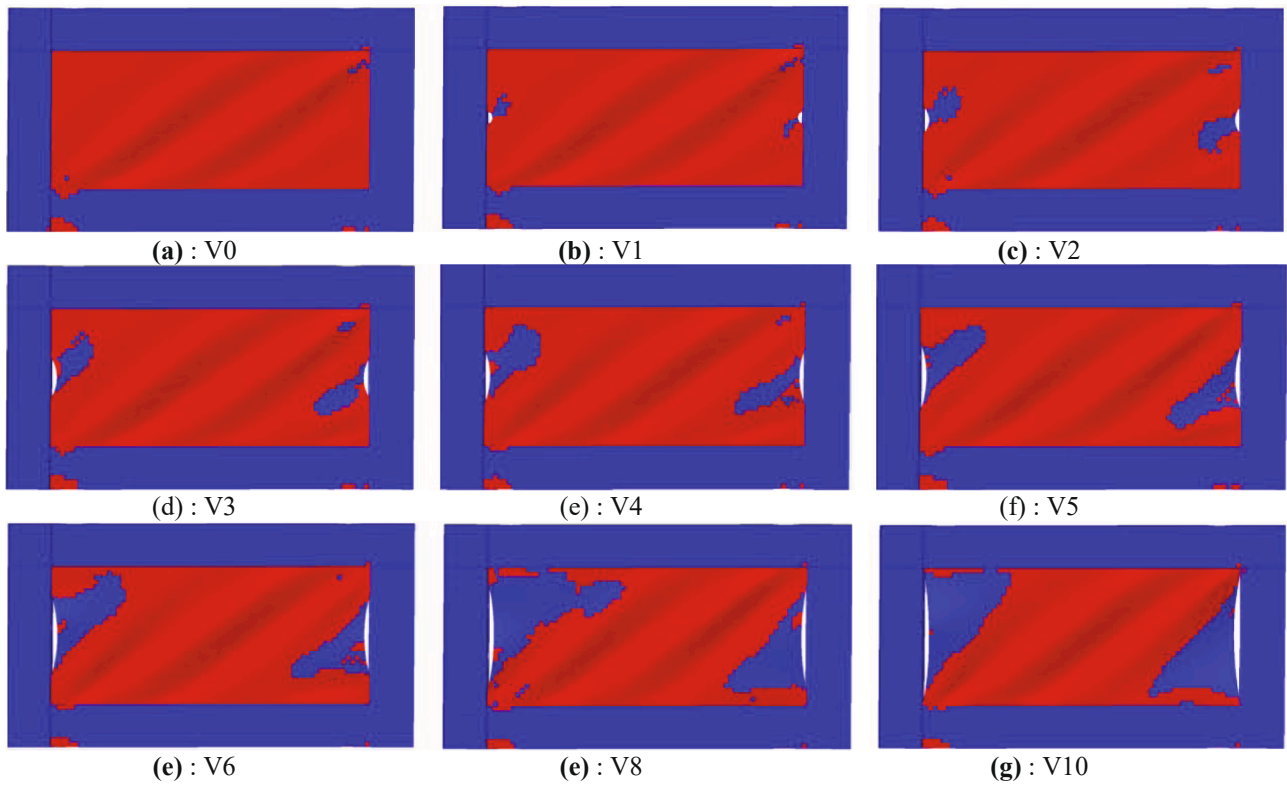


Fig. 10. The effect of the various not connected length ratios on the quality of the tension field formation in 1% total drift ratio.

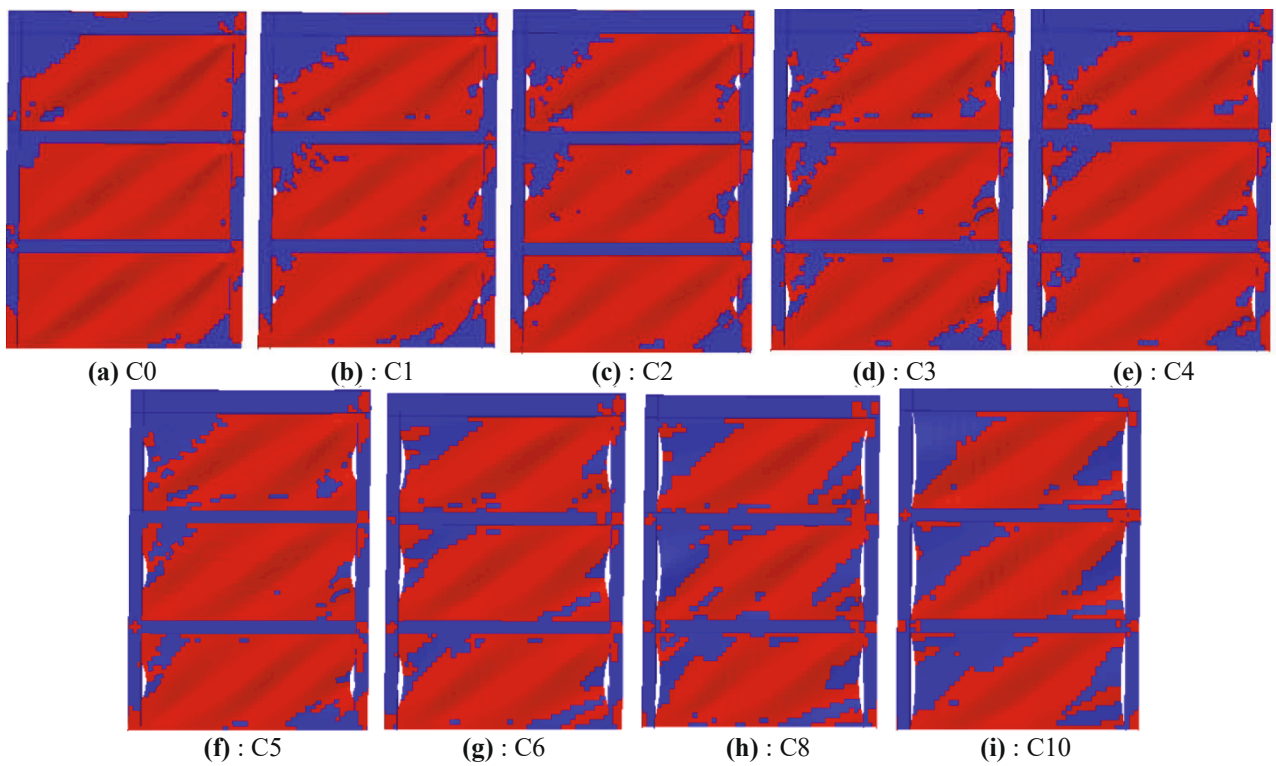


Fig. 11. The effect of the various not connected length ratios on the quality of the tension field formation in 1% total drift ratio.

(Korean Standard). The material properties were presented in Table 3. The flange and the web elements of all beams and columns satisfied the requirements for the seismic compact section according to the AISC seismic provisions (AISC341-2005).

The material properties adopted for shell elements were bilinear, incorporating the coupon yield stress and a post-yield stiffness of 0.003E [39] for web and 0.01E for boundary element material. Isotropic hardening rule was used for the analysis of both the web-

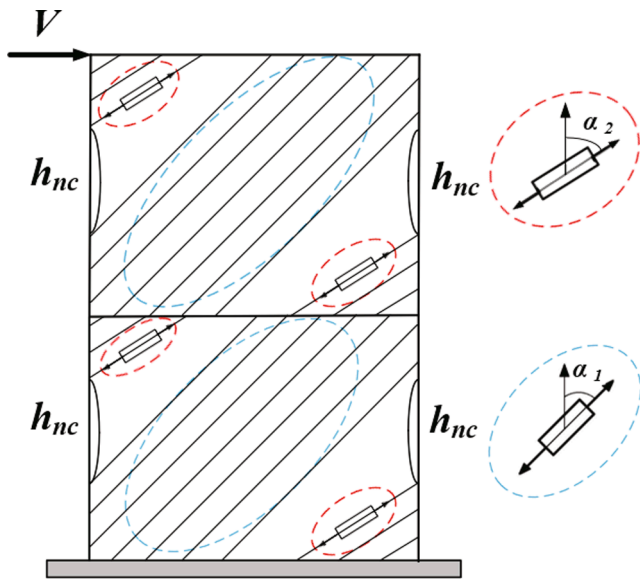


Fig. 12. Identification of two zones with different inclination of tension field strip (If  $NCR \leq 0.3$   $\alpha_1 = \alpha_2$  [31]).

plate and the boundary frame members. All mechanical properties were included in the finite element model. Both VBEs were fixed at their bases. In addition, the beams were prevented from out-of-plane displacement. It should be noted that the initial distribution of the imperfection was determined by the first buckling mode shape nodal displacement, multiplied by a small displacement amplitude of 1 mm using the Edit-Keywords in the Abaqus software. A set of mesh sensitivity analysis were conducted and a  $25 \times 25$  mm refined mesh was selected for the shell elements following a trade-off between the computational cost and the desired accuracy in accordance with the reference load–displacement results. Finally, the lateral displacement control push-over loading was applied at the top beam in horizontal direction.

Fig. 8 shows compatibility with the proper accuracy of the load–displacement behaviors between the results of the finite element modeling performed in this study and those of Choi and Park [35].

### 3. Numerical program

Based on the previous validated FEM models, twenty seven numerical finite element models with various not connected length ratio were developed for further studying the effect of this ratio on the quality of the tension field formation across the infill plate. Table 4 presents numerical codes according to the models and various not connected length ratios.

Fig. 9 to Fig. 11 shows the formation of the tension field in twenty seven numerical models in 1% total drift ratio. The red and the blue

Two-story SPSW–Lee and Tsai (2008), Aspect ratio: 0.6,  $t_w=2.6$ mm  
 Four-story SPSW–Driver (1997), Aspect ratio: 1.6,  $t_w=4.8$ mm (1st)

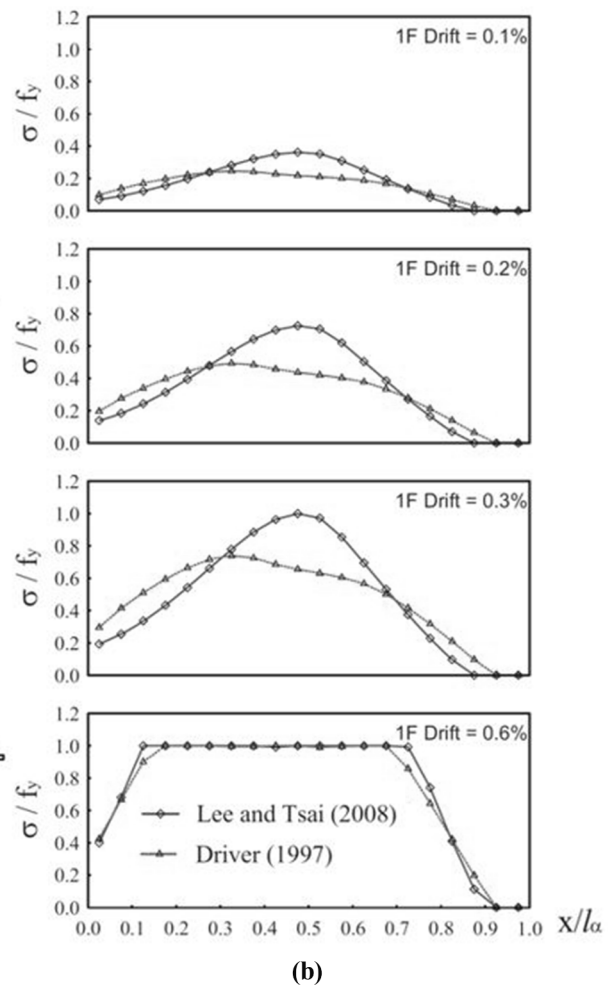
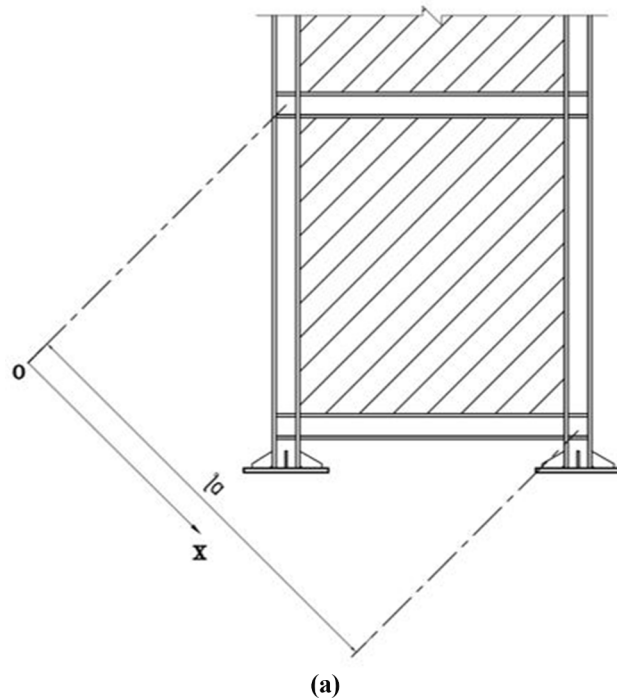


Fig. 13. Priority of plasticity development in central zone over corner zone of the first-story web plates in Lee and Tsai (2008) and Driver (1997) fully connected SPSW [40]. (a) Schematic of tension fields across the first-story web plates; (b) uniformity of panel stresses (1st) vs. percent of interstory drift ratio.

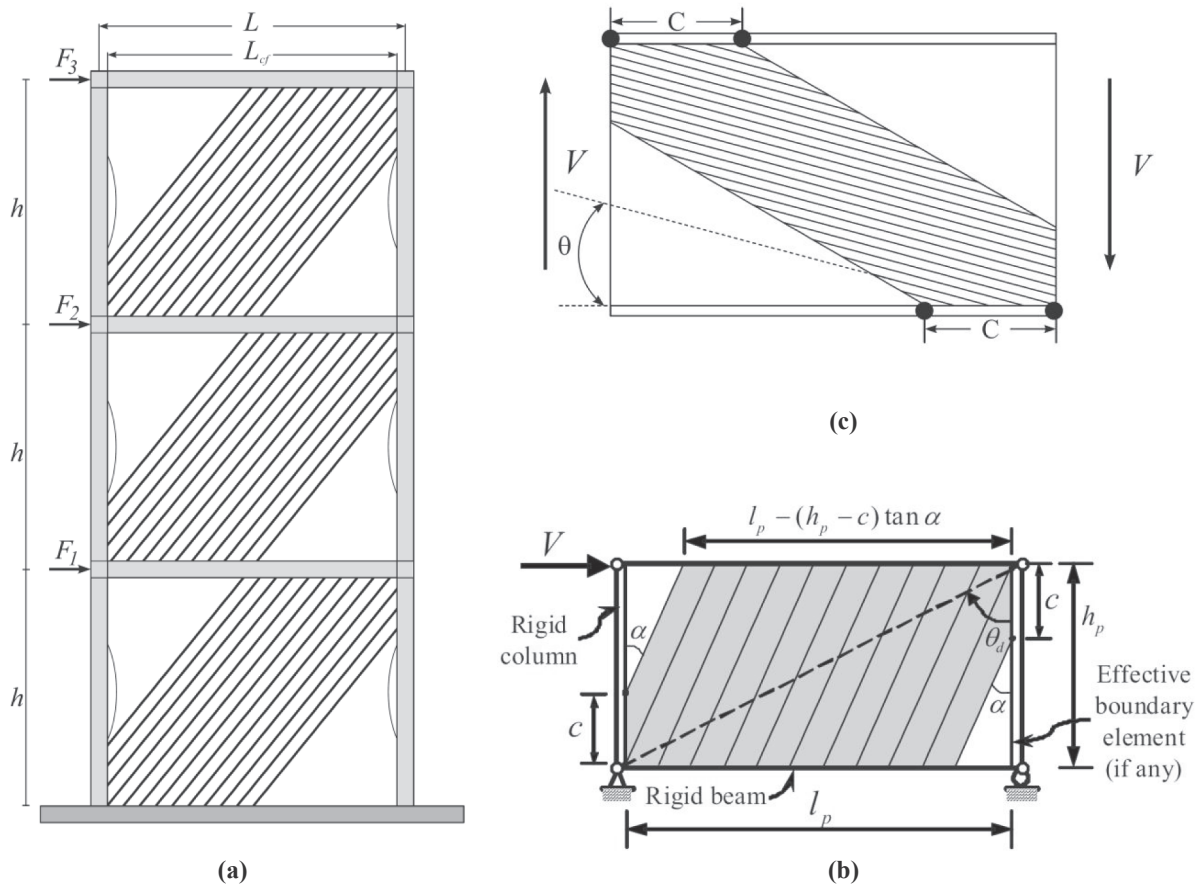


Fig. 14. Single band tension field mechanism (a) Proposed model; (b) Choi and Park [22] proposed shear wall; (c) Porter et al. [43] model for plate girder.

color represents the yield zone and the elastic zone, respectively. As it is clearly observed, the tension field's strips were formed almost parallel to each other in the first four models ( $NCR = 0\%$  to  $NCR = 30\%$ ) regardless of aspect ratio and the number of the stories. Based on this numerical study, it can be concluded that when the not connected length ratio was less than 30%, the parallelism in tension field can be used across the entire infill plate. It should be mentioned that this case was thoroughly investigated by the authors' previous study [31] for four small-scale test specimens with one story and constant aspect ratio.

However, as the not connected length ratio increased, the deviation in parallel formation of tension field's strips was clearly observed. Regarding the Fig. 9 to Fig. 11 two zones with different inclination of tension filed strip could be identified as illustrated in Fig. 12. The central zone (CE) was specified with a blue boundary line and the corner zone was shown with a red boundary line.

Qu and Bruneau [40] based on the Driver et al. (1998) [41] and Lee and Tsai (2008) [42] test specimens, showed that plasticity development in central zone occurs earlier than corner zone as depicted in Fig. 13. Fig. 13 shows stress distributions across the first-story web plates (i.e., along the direction perpendicular to the tension diagonals:  $l_a$  Path) for these two tested specimens. As it can be seen, in the middle of the path ( $X/l_a \approx 0.5$ ), which approximately represent web plate central zone there is hill, which shows priority of stress mobilization in this zone. It should be mentioned that as these two specimens were designed based on continuous connection of web plate to vertical boundary elements, therefore, as drift ratio levels progressively increase, both cases will

ultimately develop uniform tension fields.

Generally, diagonal tension strips in central zone act almost the same as a single brace between two opposite corners of the boundary frame, and make vertical truss. This truss action mechanism, prioritize plasticity development in this zone without special concern about VBE moment of inertia about an axis taken perpendicular to the plane of the web plate.

But the situations in corner zone is different, as the web plate tension is distributed across the entire vertical boundary elements length (except not connected part), so the boundary elements are subjected to bending forces. Development of plasticity in corner zone has significant dependency on several parameters such as the not connected length ratio, interstory drift ratio demand, the model's geometry, and the required VBE moment of inertia, etc. Generally, large not connected length ratio, force corner strips to mobilize in more horizontal orientation, which dramatically decreases the corner strips stiffness. Also large in-plane deflection of the VBE at the connected edges, which are located far from the central tension diagonal strips, increase this stiffness reduction. Finally this stiffness reduction leads to lower plastic strain growth, and furthermore the achievement of smaller yield zone, as illustrated in Figs. 9-11 for NCR larger than 0.3. So, it can be concluded that the increase of the not connected length ratio leads to a severe reduction in plasticity development in corner zone, which reduces the contribution of this zone in the damping of seismic input energy. Therefore, in this study it is conservatively assumed that load bearing capacity share of this zone is negligible regardless of aspect ratio and the

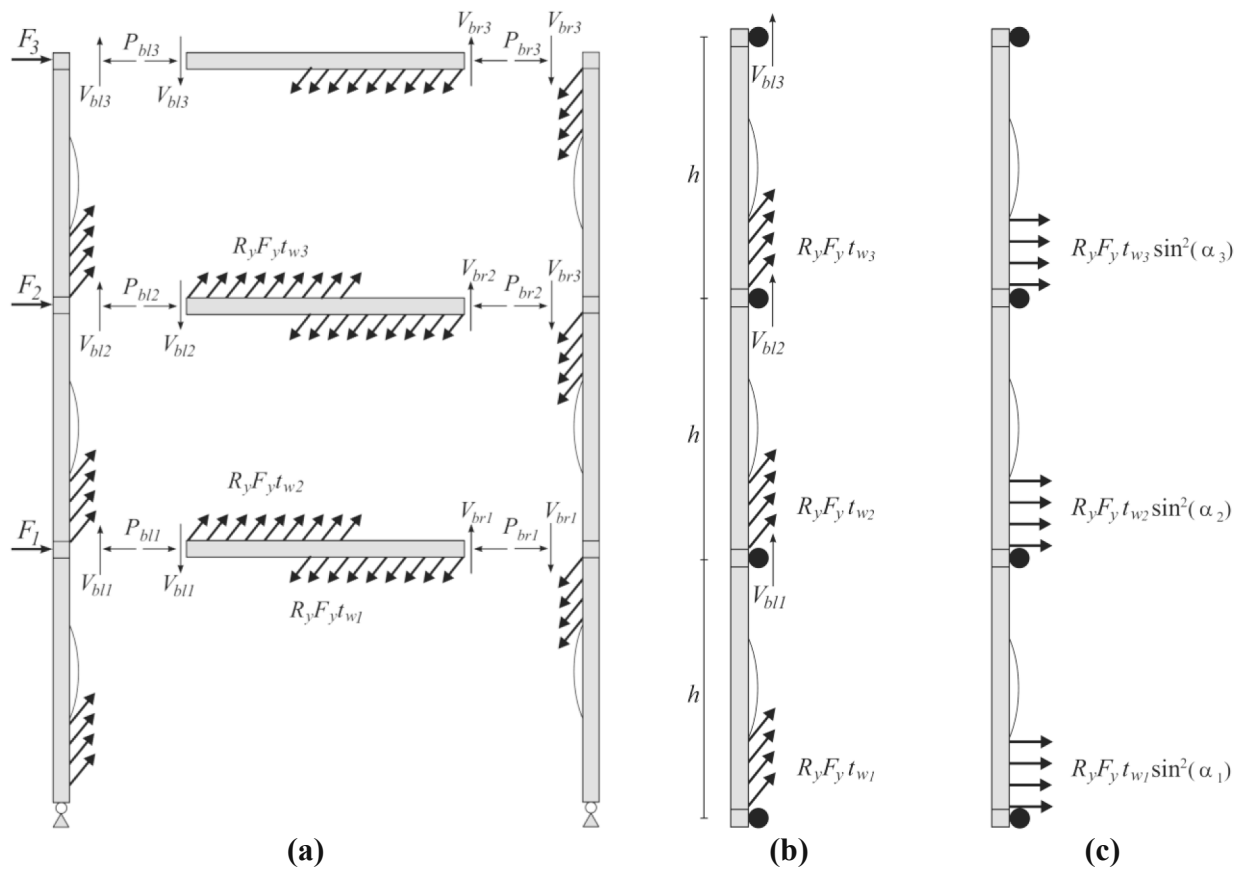


**Fig. 15.** Analytical model of proposed shear wall, (a) boundary elements internal forces; (b) VBE free body diagram; (c) Horizontal component of tension field acting along the connected part of VBE.

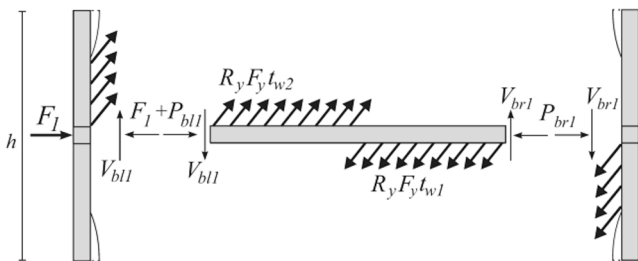


**Fig. 16.** Free-body diagram of the first story horizontal boundary element of Fig. 15 (a) shear wall.

number of the stories. According to Fig. 9 to Fig. 11, the conservative aspect of this assumption is more concerned with the intermediate range of the not connected length ( $0.3 < NCR < 0.5$ ), but for larger  $NCR$  this assumption becomes more reasonable. Effect of ignoring the corner zone contribution in load-carrying capacity are quantitatively investigated in section 5.1.

Based on the above-mentioned explanation and analogy to Choi and Park [22] work on partially connected infill plate steel shear wall and Porter et al. [43] work on plate girder, single band tension field mechanism model was proposed in this study to analyze and design of partially connected steel shear wall, which has  $NCR$  value larger than 0.3. The similarity in this analogy is that marked tension field mobilization in the corner zone of web plate is impossible owing to insufficient flexural stiffness in the central part of the flange between two stiffeners

in the plate girder [43] and the central part of the secondary boundary element in Choi and Park [22] proposed shear wall. Fig. 14 depicts single band tension field mechanism model for a three-story partially connected steel shear wall, with pin connections of the boundary elements to each other and VBE to the base.

But it should be mentioned that the model proposed by Choi and Park and Porter et al. concentrate mainly on the boundary element (End stiffener in Choi and Park proposed shear wall or flanges in Porter et al. plate girder), which does not have sufficient strength and stiffness to allow complete tension field formation across the web. This weak boundary element allows the formation of in-span plastic hinge, and therefore, are different from this study shear wall which has strong VBE, which was designed based on capacity design approach. Thus it can be concluded that the formation of single band tension field in this three models are similar, but the global mechanism, which includes plastic hinge location in boundary element is not the same.

#### 4. Prediction of structural capacity

##### 4.1. Load-carrying capacity

To obtain shear capacity of web plate in proposed shear wall, plastic analysis can be employed.

Fig. 15(a) indicates the boundary elements internal forces shown in Fig. 14(a), and Fig. 15 (b) shows the analytical model developed by Berman and Bruneau [44] which considers the VBEs to act as a continuous member over a series of supports (HBEs) spaced at story height, where a concentrated axial force component caused by

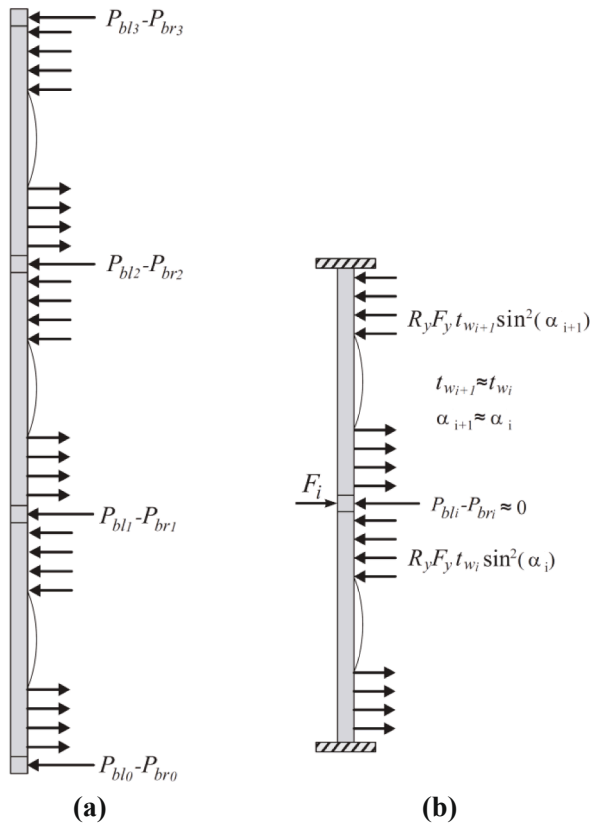


Fig. 17. Proposed simplified assumption for VBE, (a) superposition of left and right VBE, (b) considering fixed support for the top and bottom VBE end.

horizontal boundary element (HBE) shear force and distributed loading due to the formation of a diagonal tension field in the infill plate are applied to VBE. This distributed load occurs at angle  $\alpha$  from the vertical axis, with an intensity of  $R_y F_y t_w$  (where  $R_y$  is the ratio of mean to nominal yield stress of the web plate,  $F_y$  is the web plate yield stress and  $t_w$  is the infill plate thickness). This distributed loading can be decomposed to horizontal and vertical components acting along the VBE. Fig. 15(c) depicts horizontal component of this distributed load which is acting along the connected part of VBE. Fig. 16. illustrates free-body diagram of the first story horizontal boundary element of Fig. 15(a) shear wall.

Using equilibrium equation in horizontal direction (Eq. (1)), and manipulating the related term, finally the first story applied lateral force ( $F_1$ ) could be calculated as presented in Eq. (2).

$$\sum F_X = 0 \Rightarrow F_1 + P_{bl1} + \left( 0.5R_y F_y t_w \left( L_{cf} - \left( \frac{h+h_{nc}}{2} \right) \tan\alpha \right) \sin 2\alpha \right)_{2nd} = \left( 0.5R_y F_y t_w \left( L_{cf} - \left( \frac{h+h_{nc}}{2} \right) \tan\alpha \right) \sin 2\alpha \right)_{1st} + P_{br1} \tag{1}$$

$$F_1 = \left( 0.5R_y F_y t_w \left( L_{cf} - \left( \frac{h+h_{nc}}{2} \right) \tan\alpha \right) \sin 2\alpha \right)_{1st} - \left( 0.5R_y F_y t_w \left( L_{cf} - \left( \frac{h+h_{nc}}{2} \right) \tan\alpha \right) \sin 2\alpha \right)_{2nd} + P_{br1} - P_{bl1} \tag{2}$$

Based on this approach we can derive similar equations for other stories applied lateral forces as follows:

$$F_2 = \left( 0.5R_y F_y t_w \left( L_{cf} - \left( \frac{h+h_{nc}}{2} \right) \tan\alpha \right) \sin 2\alpha \right)_{2nd} - \left( 0.5R_y F_y t_w \left( L_{cf} - \left( \frac{h+h_{nc}}{2} \right) \tan\alpha \right) \sin 2\alpha \right)_{3rd} + P_{br2} - P_{bl2} \tag{3}$$

$$F_3 = \left( 0.5R_y F_y t_w \left( L_{cf} - \left( \frac{h+h_{nc}}{2} \right) \tan\alpha \right) \sin 2\alpha \right)_{3st} + P_{br3} - P_{bl3} \tag{4}$$

As similar structural sections are used in left and right vertical boundary element in steel shear wall, by using Berman and Bruneau [44] approach presented in Fig. 15(b) and (c), the difference between the value of HBE right and left axial force ( $P_{blr}-P_{bri}$ ) could be calculated by applying the principle of superposition as illustrated in Fig. 17(a). To simplify final formulation, extra assumptions below are made.

- Considering the top and bottom column end to act as a member with fixed support.
- Two adjacent story earthquakes induced shear action ( $F_i$ ) for usual load cases have minor differences as a result, distributed loading due to the formation of a diagonal tension field in this two adjacent story infill plates ( $R_y F_y t_w$  &  $\alpha_i$ ) can be considered equal (Similar to Timler and Kulak [45] study).

Taking these assumptions into perspective, according to Fig. 17 (b), regarding to symmetric structure and anti-symmetric loading, it can be concluded that, above-mentioned value ( $P_{blr}-P_{bri}$ ) is almost equal to zero for intermediate story, and conservatively could be neglected for top story owing two strut action of top HBE. Finally probable shear strength of web plate can be obtained by summation of stories applied lateral forces.

$$V = F_1 + F_2 + F_3 = \left( 0.5R_y F_y t_w \left( L_{cf} - \left( \frac{h+h_{nc}}{2} \right) \tan\alpha \right) \sin 2\alpha \right) \tag{5}$$

The nominal shear strength of web plate can be calculated without the material factor  $R_y$  as presented in Eq. (6).

$$V_n = F_1 + F_2 + F_3 = \left( 0.5F_y t_w \left( L_{cf} - \left( \frac{h+h_{nc}}{2} \right) \tan\alpha \right) \sin 2\alpha \right) \tag{6}$$

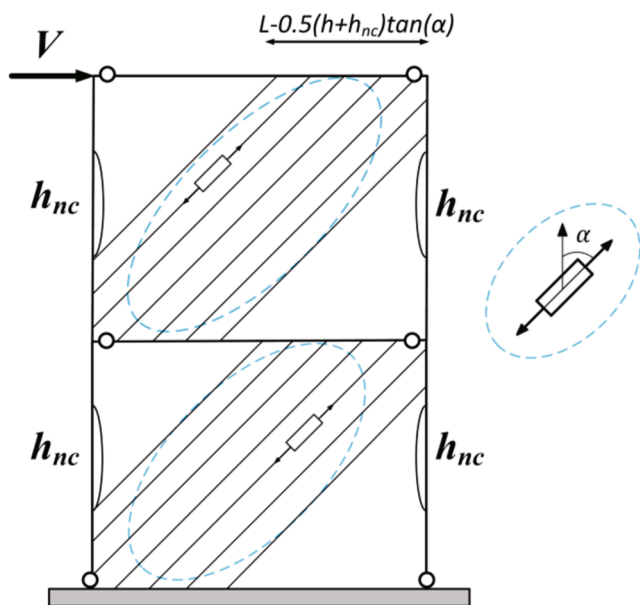


Fig. 18. Idealized tension-strip model for the prediction of the inclination angle of the proposed shear wall.

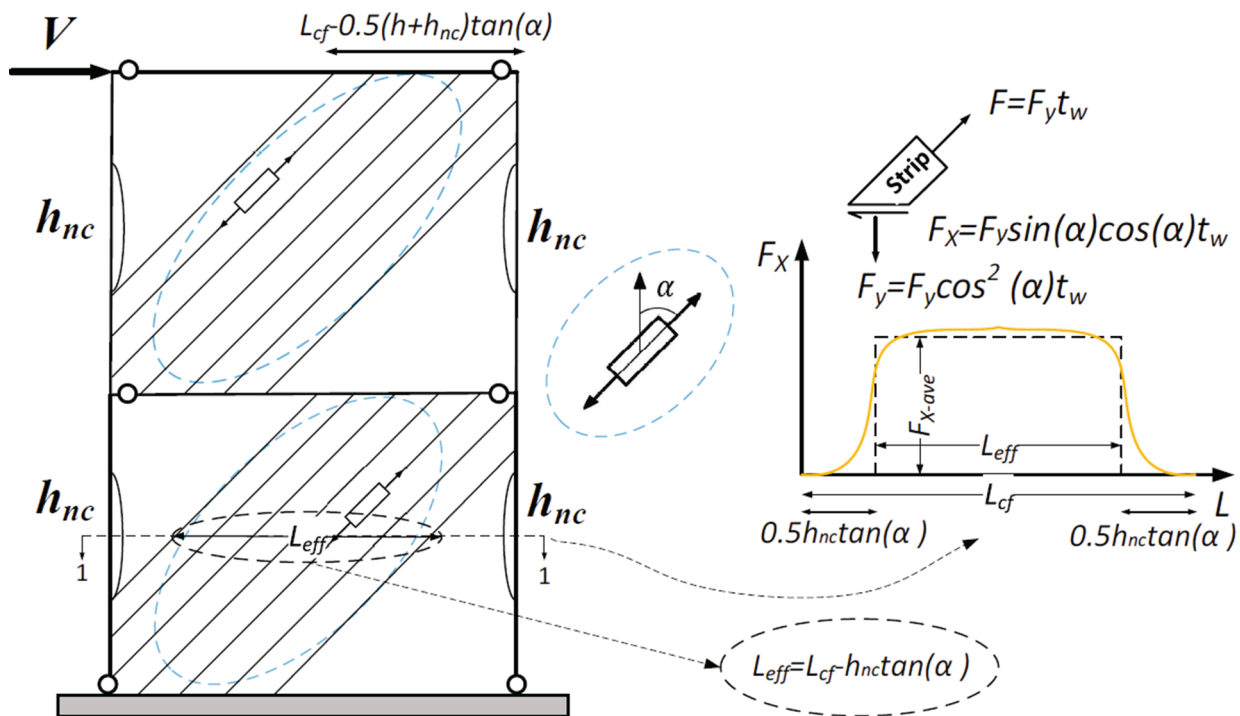


Fig. 19. Schematic representation of stress mobilization (shear flow) in web plate of under study steel shear wall (P.M.).

#### 4.2. Inclination angle of tension field

A derivation for the inclination angle of tension field within the infill plate of an unstiffened shear wall subjected to transverse loading was first introduced by Thorburn and Kulak in 1982 [1], using least work method. According to their study, infill plates, which buckles early under cyclic shear load can be modeled as a series of parallel pin-ended tension strips inclined at angle  $\alpha$ . This investigation was followed by Timler and Kulak in 1984 [45]. The CAN/CSA-S16-94 [46], and the AISC-341 2005 [36] adopt Timler and Kulak work presented by Eq. (7).

$$\tan^4(\alpha) = \frac{1 + \frac{t_w L}{2A_c}}{1 + t_w h \left( \frac{1}{A_b} + \frac{h^3}{360I_c L} \right)} \quad (7)$$

where  $h$  = story height;  $L$  = center-to-center distance between the boundary columns;  $t_w$  = thickness of the infill plate;  $A_b$  and  $A_c$  = cross-sectional areas of the beam and column, respectively; and  $I_c$  = moment of inertia of the boundary column. As beam and column cross-sectional area ( $A_b$  &  $A_c$ ) and moment of inertia of the column ( $I_c$ ) increase, the inclination angle of the tension field ( $\alpha$ ) converges to  $45^\circ$ .

Work expression derived by Timler and Kulak [45] includes stored strain energy caused by axial forces within the system and column bending considering an assumed uniform tension field within the plate (series of parallel tension strips). But generally, in steel plate shear walls with thin infill plates, beams and columns are designed to have sufficient stiffness and strength to resist the tension field force of the infill plates. Therefore, the frame members can be modeled as rigid boundaries. Thus, the inclination angle of the tension field can be calculated by considering merely the effective tension field area of the infill plate [22]. On the other hand, in the steel plate walls with partially connected infill plates or a wall opening, the tension field is not uniformly distributed across the infill plate. The inclination angle of the tension field should be determined by considering the effective tension field area.

Fig. 18 shows an idealized tension-strip model for the prediction of the inclination angle of the steel plate shear walls with partial length connection to vertical boundary element with  $NCR$  value larger than 0.3. In this model hinge connections were used at the beam-to-column connections. This is because rigidity of the connection between the beam and column does not affect the internal work of the tension strips of the infill plate [22]. As mentioned, the infill plate can be modeled with a series of tension strips inclined at an angle  $\alpha$ .

Based on the Eq. (6),  $\sigma$  is calculated and presented as follows:

$$\sigma = \frac{V}{t_w \left( L - \left( \frac{h+h_{nc}}{2} \right) \tan \alpha \right) \sin \alpha \cos \alpha} \quad (8)$$

It should be mentioned that the total shear  $V$  induced by lateral load is assumed to be merely withstood by the infill plate.

The strain energy stored in infill plate due to membrane force is as follows:

$$W_{Total} = W_{Web-nc} = \int \frac{\sigma^2}{2E} t_w dA \quad (9)$$

where  $A$  = effective tension field area, which is defined below:

$$A = Lh - 2 \times \left( \frac{h+h_{nc}}{2} \right) \left( \frac{h+h_{nc}}{2} \right) \tan \alpha = Lh - \frac{(h+h_{nc})^2}{4} \tan \alpha \quad (10)$$

Finally, the internal work done by the panel under a tension field stress is calculated as follows:

$$W_{Total} = W_{Web-nc} = \frac{V^2 \left( Lh - \frac{(h+h_{nc})^2}{4} \tan \alpha \right)}{2Et_w \left( L - \left( \frac{h+h_{nc}}{2} \right) \tan \alpha \right)^2 \sin^2(\alpha) \cos^2 \alpha} \quad (11)$$

According to the least work principle, the critical value of  $\alpha$  is obtained by minimizing the work done by differentiating with respect to  $\alpha$

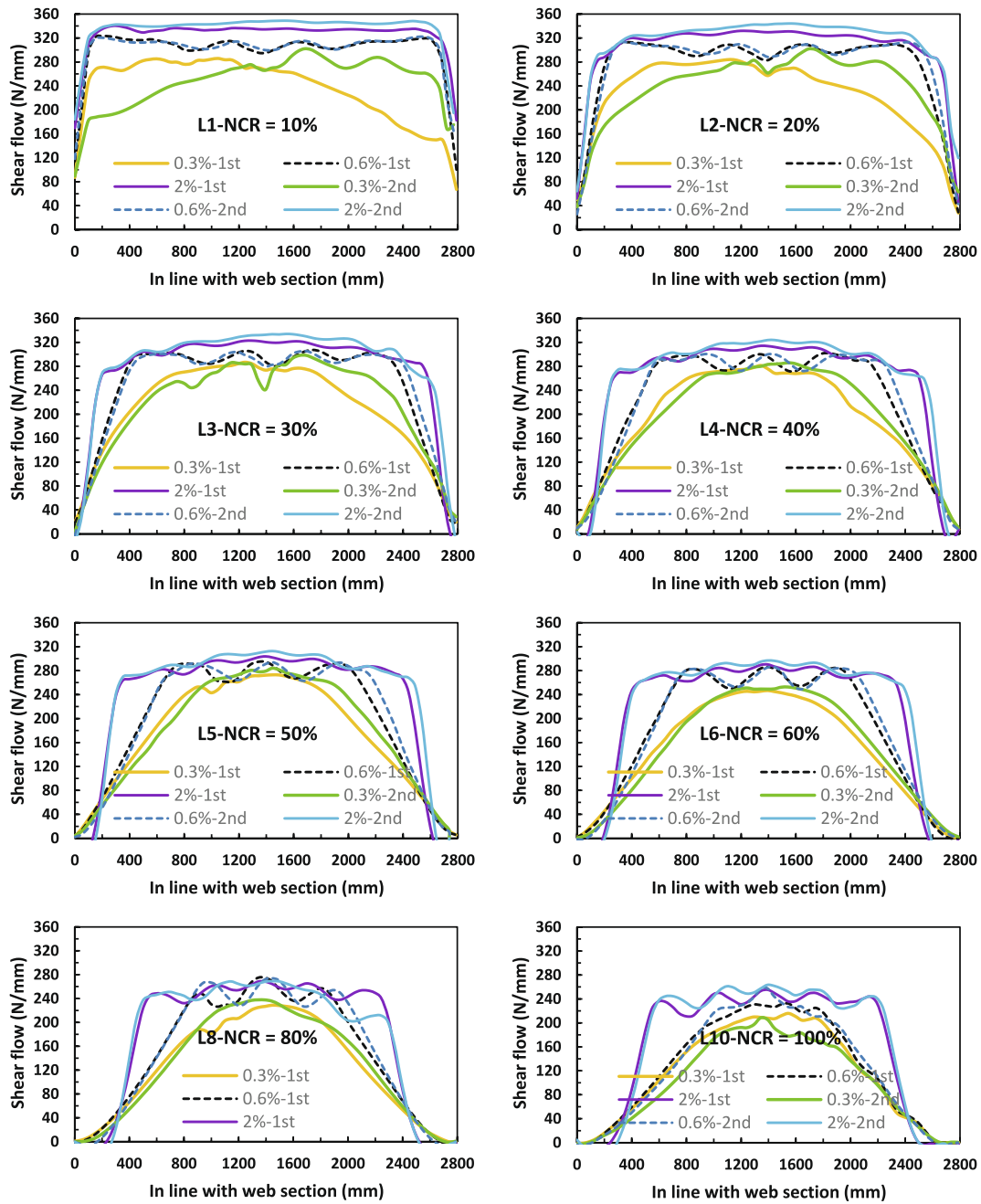


Fig. 20. Shear flow due to tension field stress along the web plate section cut with respect to percent of total drift ratio based on Li et al. reference model; (a) L1; (b) L2; (c) L3; (d) L4; (e) L5; (f) L6; (g) L8; (h) L10 for 1st & 2nd story.

and equating the result to zero.

$$\frac{\partial W_{Total}}{\partial \alpha} = 0 \tag{12}$$

$$\Rightarrow \frac{d}{d\alpha} \left( \frac{V^2}{2E} \left( \frac{Lh - \frac{(h+h_w)^2}{4} \tan \alpha}{t_w \left( L - \left( \frac{h+h_w}{2} \right) \tan \alpha \right)^2 \sin^2(\alpha) \cos^2 \alpha} \right) \right) = 0$$

After deriving differentiated terms and manipulating them (presented in Eq. (13)) into achieving a simplified equation, a fourth order equation (Eq. (14)) is obtained in terms of  $\tan(\alpha)$  with constant coefficients (Eq. (15)).

$$\begin{aligned} & (0.5 + 0.5NCR)^3 \tan^4(\alpha) - 3 \left( \frac{L}{h} \right) (0.5 + 0.5NCR)^2 \tan^3(\alpha) \\ & - \left( 3(0.5 + 0.5NCR)^3 - 2 \left( \frac{L}{h} \right)^2 \right) \tan^2(\alpha) \\ & + \left( \left( \frac{L}{h} \right) (4.5 + 0.5NCR)(0.5 + 0.5NCR) \right) \tan(\alpha) - 2 \left( \frac{L}{h} \right)^2 = 0 \end{aligned} \tag{13}$$

$$A \tan^4(\alpha) + B \tan^3(\alpha) + C \tan^2(\alpha) + D \tan(\alpha) + E = 0 \tag{14}$$

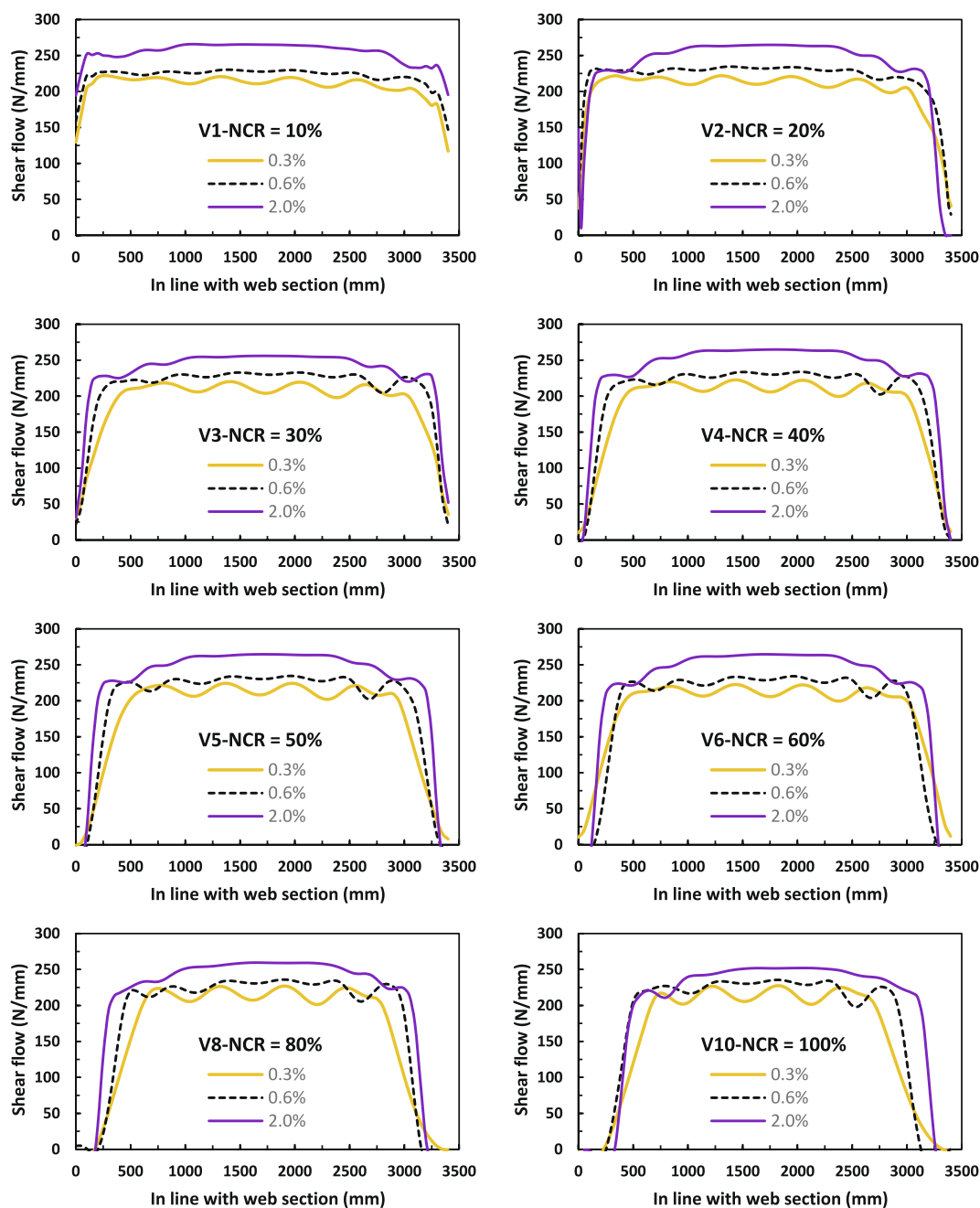


Fig. 21. Shear flow due to tension field stress along the web plate section cut with respect to percent of total drift ratio based on Vian et al. reference model; (a) V1; (b) V2; (c) V3; (d) V4; (e) V5; (f) V6; (g) V8; (h) V10.

$$\begin{aligned}
 A &= (0.5 + 0.5NCR)^3, \quad B = -3\left(\frac{L}{h}\right)(0.5 + 0.5NCR)^2, \\
 C &= -\left(3(0.5 + 0.5NCR)^3 - 2\left(\frac{L}{h}\right)^2\right), \quad D = \left(\left(\frac{L}{h}\right)(4.5 + 0.5NCR)(0.5 + 0.5NCR)\right), \\
 E &= -2\left(\frac{L}{h}\right)^2
 \end{aligned}
 \tag{15}$$

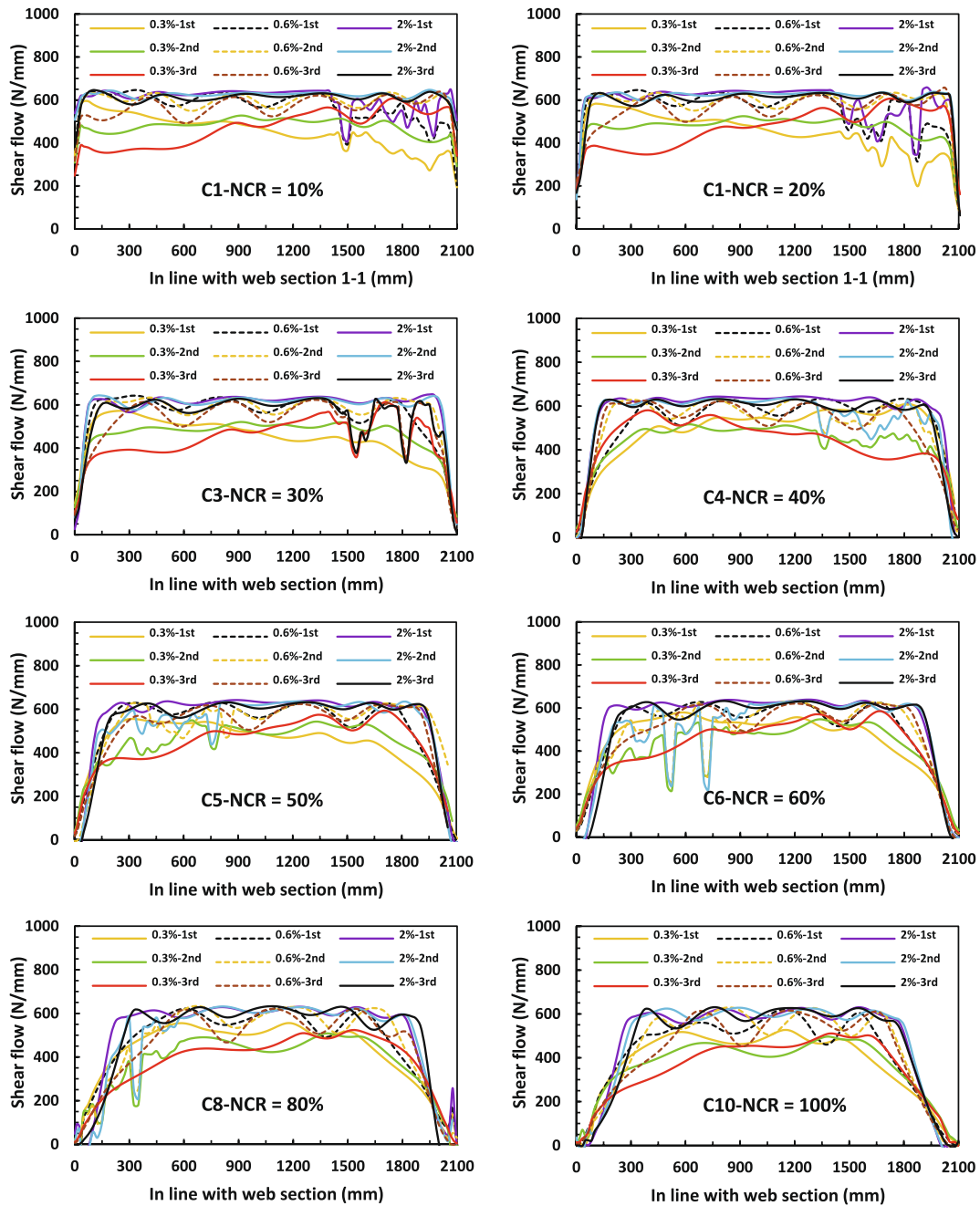


Fig. 22. Shear flow due to tension field stress along the web plate section cut with respect to percent of total drift ratio based on Choi and Park reference model; (a) C1; (b) C2; (c) C3; (d) C4; (e) C5; (f) C6; (g) C8; (h) C10 for 1st, 2nd & 3rd story.

Table 5

Comparison with mobilized web plate shear force based on finite element model (Actual) and proposed model distribution.

NCR (%)	Li et al.			Vian et al.			Choi and Park		
	P.M.(kN)	FEM (kN)	Error (%)	P.M. (kN)	FEM (kN)	Error (%)	P.M. (kN)	FEM (kN)	Error (%)
40%	564	531.5	-6.1	634.2	636.3	0.3	1094.8	1026.1	-6.7
50%	513.5	488.1	-5.2	609.2	615.6	1	1049.2	1001.0	-4.8
60%	463.8	418.3	-10.9	584.9	635.4	7.9	1004.8	962.1	-4.4
80%	372.8	350.4	-6.4	537.7	556.0	3.3	918.5	890.5	-3.2
100%	327	317.5	-3.0	491.3	527.9	6.9	833.6	801.1	-4.0

5. Proposed analytical model

Based on the aforementioned description, Fig. 19 schematically

depicts stress (shear flow) distribution in infill plate of previously described steel shear walls (NCR > 0.3) in time of web plate plastic mechanism formation. This simplified proposed model (P.M.) assumes

**Table 6**

Value of tension field inclination angle and interstory drift ratio in time of yielding.

NCR	Li et al.		Vian et al.		Choi and Park	
	$\alpha$ (deg)	$\gamma_y$	$\alpha$ (deg)	$\gamma_y$	$\alpha$ (deg)	$\gamma_y$
40%	28.8	0.0026	37.6	0.0017	37.8	0.003
50%	28.2	0.0026	37.3	0.0017	37.5	0.0031
60%	27.6	0.0027	37.1	0.0017	37.3	0.0031
80%	26.7	0.0027	36.5	0.0017	36.9	0.0031
100%	26.3	0.0027	36.5	0.0017	36.7	0.0031

that almost uniform distributed shear load was mobilized along the effective length of web plate central section ( $L_{eff}$ ) which is called single band model in this article. It should be mentioned that this proposed model assumes that there is plastic plateau after yield stress of steel material to postpone hardening effect.

Fig. 20 to Fig. 22 illustrate the distributed shear load intensity due to tension field stress ( $\sigma_{12} \times t_w = \text{shear flow}$ ) along the web plate cross section cut (Section 1-1 in Fig. 19) with respect to percent of interstory drift ratio. As it can be obviously witness, shear flow follows the plateau-shaped distribution, which means that the lion's share of stress is mobilized in width of this plateau, and an increase in drift ratio leads to complete this distribution shape.

To validate Fig. 19 representation of stress distribution, Table 5 compares the mobilized web plate shear force (Section 1-1 in Fig. 19) based on finite element models (Fig. 20 to Fig. 22) which equals to

covered area under shear flow graph and proposed model distribution in 0.3% interstory drift ratio. It should be mentioned that proposed model mobilized shear force is equal to effective length of web plate central section ( $L_{eff}$ ) multiplied by average value of shear flow ( $F_x = F_{x-ave}$  in Fig. 19), which is calculated based on Eq.

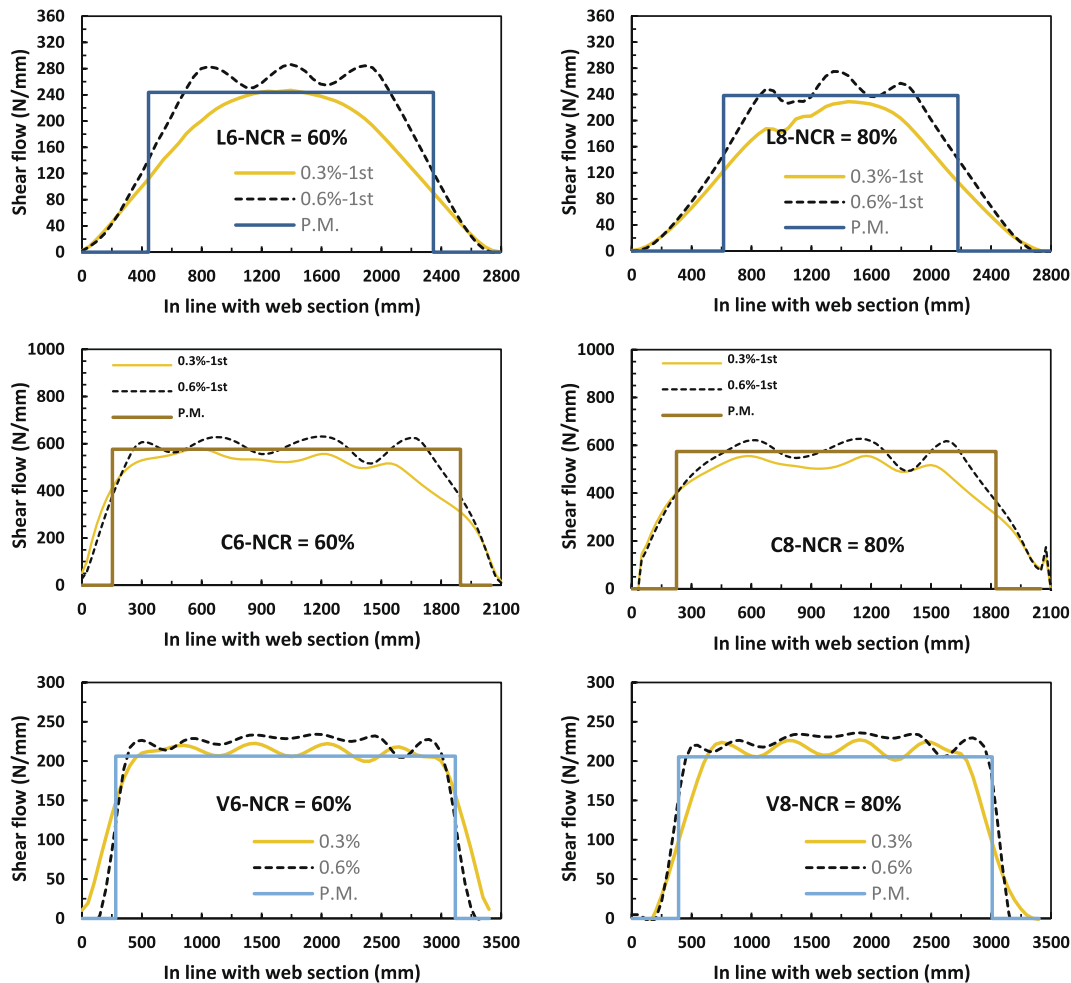
$$V_{web-P.M.} = (L_{cf} - L_{NEFF}) \times (F_y \sin(\alpha) \cos(\alpha) t_w) \tag{16}$$

Table 6 represents the value of tension field inclination angle based on Eq. (14), which is utilized to calculate P.M. mobilized shear forces in web plate central section (Table 5) and the interstory drift angle in which the web plate would start to yield based on Eq. (17) [47].

$$\gamma_y = \frac{2\epsilon_y}{\sin(2\alpha)} \tag{17}$$

According to Table 6, 0.3% drift ratio (equal to 0.003 drift angle) led to yielding in web plate of all models and, therefore, was an appropriate value to verify the proposed model mobilized shear force.

It is worthy of mention that Eq. (17) was developed based on the assumption that all active strips mobilized simultaneously in the same stress level, but actually as described before (Fig. 13) when drift ratio levels gradually increase, uniform tension fields will ultimately develop across the active area of infill plate. Therefore, it can be concluded that above equation predicts the occurrence of yielding in mid part of the central zone, which mobilizes truss action. Thus the development of fully yield single band requires time for increase in drift as well as stress redistribution. As a result, in lower drift, the proposed method may does not have good shape accordance with plateau shape distribution, which



**Fig. 23.** Accordance between proposed and finite element model shear flow distribution in line with 1st web central section; (a) L6; (b) L8; (c) C6; (d) C8; (e) V6; (f) V8 for 1st story.

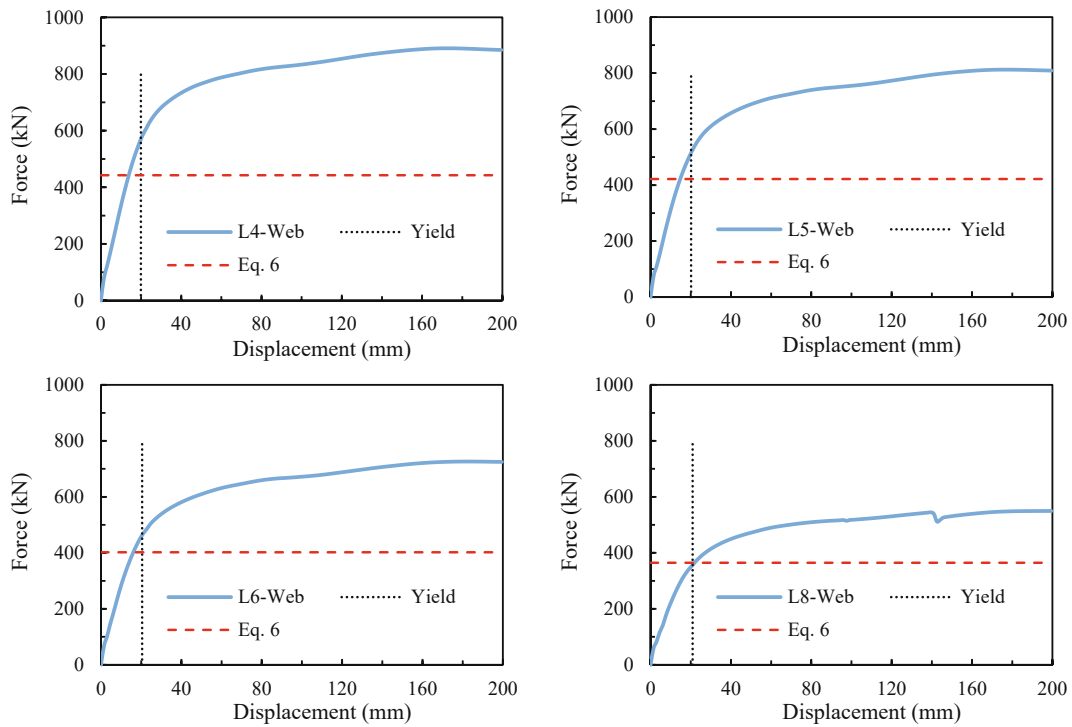


Fig. 24. Actual value of shear strength in web plate resulted from Abaqus, in comparison with predicted value (Eq. (5)) based on Li et al. reference model; (a) L4; (b) L5; (c) L6; (d) L8.

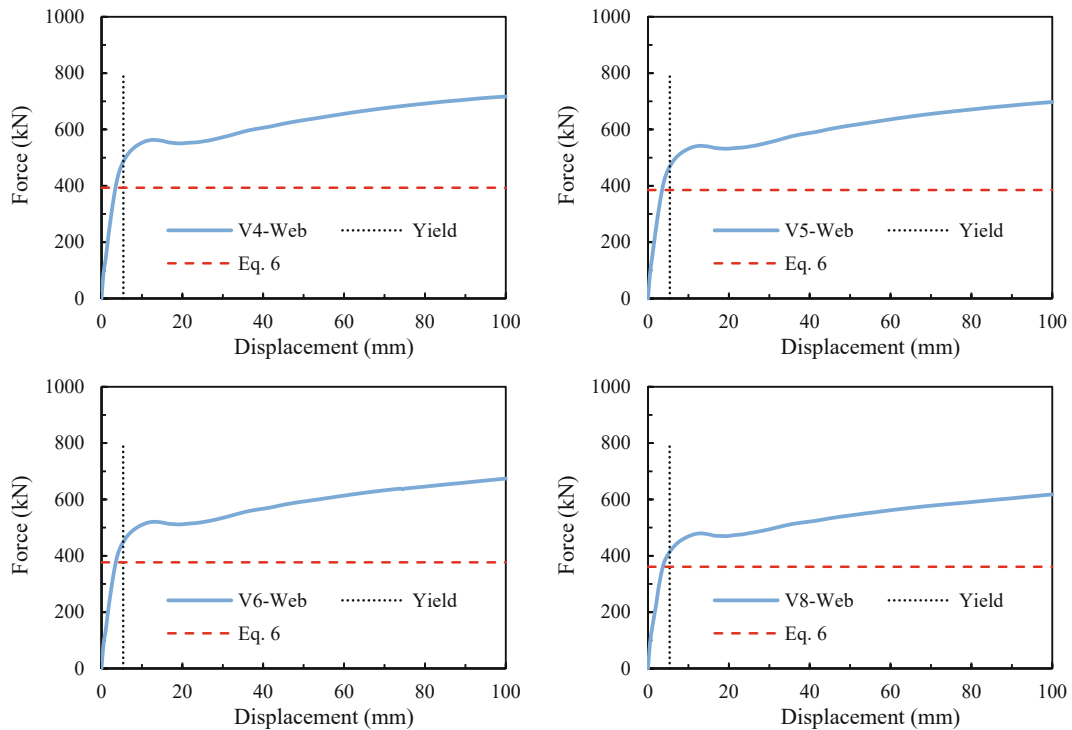


Fig. 25. Actual value of shear strength in web plate resulted from Abaqus, in comparison with predicted value (Eq. (6)) based on Vian et al. reference model; (a) V4; (b) V5; (c) V6; (d) V8.

assumes that almost uniform distributed shear load was mobilized along the effective length of web plate central section ( $L_{eff}$ ), but as drift increases, shear flow, almost complies with the corresponding distribution.

To consider the effect of increase in interstory drift on improved

compliance, as an example, Fig. 23 illustrates the accordance between proposed and finite element model shear flow distribution in line with 1st web central section (arbitrary selection) for 0.3% & 0.6% inter story drift ratio. As it can be obviously observed, increasing interstory drift ratio from 0.3% to 0.6% led to better conformance between distribution

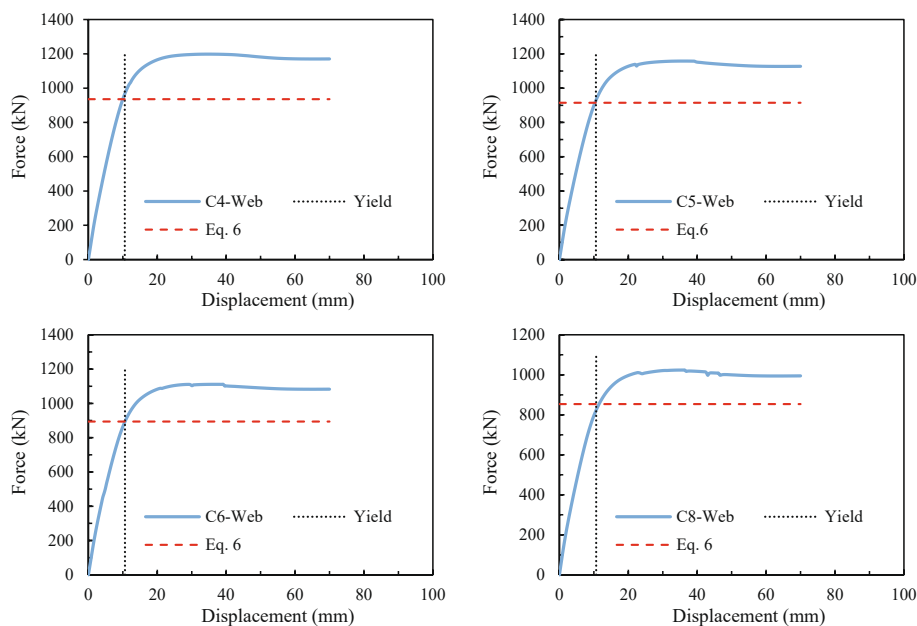


Fig. 26. Actual value of shear strength in web plate resulted from Abaqus, in comparison with predicted value (Eq. (6)) based on Choi and Park. reference model; (a) C4; (b) C5; (c) C6; (d) C8.

Table 7

Comparison between web plate shear strength based on finite element model (Actual) and predicted value (Eq. (6)).

NCR (%)	Li et al.			Vian et al.			Choi and Park		
	Eq. (6) (kN)	FEM (kN)	Error (%)	Eq. (6) (kN)	FEM (kN)	Error (%)	Eq. (6) (kN)	FEM (kN)	Error (%)
40%	442.5	569.4	-22	393.2	486.2	-19	935.7	966.8	-3.2
50%	421.7	515	-18	385.1	469	-17.9	914.8	928.5	-1.5
60%	402.1	462.9	-13	376.8	448.8	-16	894.1	893.9	0
80%	364.6	356.2	2	361.1	413.6	-12.7	853.6	823.4	3.7
100%	326.8	327.6	0	344.8	392.9	-12.24	812.8	760.2	6.9

shape of shear flow in proposed and finite element model. Ultimately it should be mentioned that regardless of shape distribution conformity, proposed method predicts mobilized shear force in web central section with proper accuracy.

Based on the above-mentioned description, it can be concluded that proposed model shows reasonable error in presenting of tension field in web plate central zone of this study steel shear wall ( $NCR > 0.3$ ).

5.1. Verification shear strength derived

In this section the ability of derived shear strength relation (Eq. (6)) to predict structural capacity of partially connected steel shear wall with large value of not connected length ratio ( $NCR \geq 0.3$ ) were investigated based on finite element modeling results. Seismic design provisions [10] mandate the web plates to provide 100% of the required shear strength and save a boundary frame capacity as a compensator of web plate improper seismic behavior (tension only). Thus in this study numerical web plate force-displacement diagrams were derived by subtracting wall force-displacement diagrams from that of frame force-displacement as illustrated in Fig. 24 to Fig. 26. Actual yield strength is defined by intersecting vertical dotted lines (which is determined based on Eq. (17)) and web plate force-displacement diagrams. As it can be visually observed, the predicted (Eq. (6)) and actual yield strength value based on numerical model are in reasonable accordance. Table 7 quantitatively compares this value. As it can be seen Eq. (6) determines the shear yield strength of the proposed steel wall with a good accuracy. Ignoring the contribution of corner zone to load-carrying capacity does not have significant effect on this prediction, but as expected, this prediction is to

some extent conservative for the intermediate range of the not connected length ( $0.3 < NCR < 0.5$ ).

6. Conclusions

In this research project analytical studies were conducted based on numerical evidence so as to investigate the effects of large value of not connected length ratio of infill plate to middle height of vertical boundary element ( $NCR \geq 0.3$ ) on the quality of tension field formation in presence of panel aspect ratio and number of stories variation. The most important results of this research project are outlined below.

- (1) Based on numerical evidence and analogy to previous work of steel plate shear wall and plate girder, simplified proposed model named “single band tension field mechanism” was introduced.
- (2) Relative accordance between proposed and finite element model shear flow distribution corroborates that panel aspect ratio and the number of stories variation have no significant effect on proposed method and corresponding governing equation.
- (3) Shear strength of the infill plate (with the limit state of shear yielding) was determined, and numerically validated. The proposed equation was derived using the plastic analysis of the single band tension field mechanism model.
- (4) Inclination angle of the tension field within the infill plate of an unstiffened shear wall subjected to transverse loading is derived using the least work principle, and was numerically validated.

## Declaration of Competing Interest

The authors declare that they have no known competing financial interests or personal relationships that could have appeared to influence the work reported in this paper.

## References

- [1] Thorburn L-J, Kulak G-L & Montgomery C-J. Analysis of steel plate shear walls, Structural Engineering Report No. 107, Department of Civil Engineering, University of Alberta, Edmonton, 1983.
- [2] Tromposch E-W. Cyclic and static behavior of thin panel steel plate shear walls. Ph. D. Dissertation, Department of Civil Engineering, University of Alberta, Edmonton, 1987.
- [3] Roberts T-M, Sabouri-Ghomi S. Hysteretic characteristics of unstiffened plate shear panels. *Thin-Walled Struct* 1991;12(2):145–62.
- [4] Caccese V, Elgaaly M, Chen R. Experimental study of thin steel-plate shear walls under cyclic load. *J Struct Eng* 1993;119(2):573–87.
- [5] Hajmirsadeghi M, Mirtaheri M, Zandi A-P, Hariri-Ardebilil M-A. Experimental cyclic test and failure modes of a full scale enhanced modular steel plate shear wall. *Eng Fail Anal* 2019;95:283–8.
- [6] Gorji Azadariani M, Gholhaki M, Kafi M-A. Hysteresis finite element model for evaluation of cyclic behavior and performance of steel plate shear walls (SPSWs). *Structures* 2021;29:30–47.
- [7] Lubell A-S, Prion H-G, Ventura C-E, Rezaei M. Unstiffened steel plate shear wall performance under cyclic loading. *J Struct Eng* 2000;126(4):453–60.
- [8] Broujerdian V, Ghamari A, Abbaszadeh A. Introducing an efficient compound section for steel shear wall using flat and corrugated plates. *Structures* 2021;33:2855–71.
- [9] Berman J-W, Lowes L-N, Okazaki T, Bruneau M, Tsai K-C, Driver R-G, Sabelli R, and Moore W-P. Research needs and future directions for steel plate shear walls. In *Proceeding of the 2008 Structures Congress*.
- [10] AISC. Seismic provisions for structural steel buildings. ANSI/AISC 341–16, American Institute of Steel Construction, Chicago, IL, 2016.
- [11] Chen S-J, Jhang C. Cyclic behavior of low yield point steel shear walls. *Thin-Walled Struct* 2006;44(7):730–8.
- [12] Matteis G-De, Mazzolani F, Panico S. Experimental tests on pure aluminum shear panels with welded stiffeners. *Eng. Struct.* 30 (6) (2008) 1734–1744.
- [13] Baftechi H. Analytical and experimental study of aluminum shear panels for retrofitting of existing structures. M.Sc. Thesis, K.N. Toosi University of Technology, Tehran, Iran, 2014.
- [14] Vian D, Bruneau M. Steel plate walls for seismic design and retrofit of building structures. Technical Report MCEER-05-0010, Multidisciplinary Center for Earthquake Engineering Research. Buffalo, NY: State University of New York at Buffalo; 2005.
- [15] Li C-H, Tsai K-C, Lin C-H, Chen P-C. Cyclic tests of four two story narrow steel plate shear walls. Part 2: experimental results and design implications. *J Earthquake Eng Struct Dyn*, 39 (7) (2010) 801–826.
- [16] Jahanpour A, Jonson J, Moharrami H. Seismic behavior of semi-supported steel shear walls. *J Constr Steel Res* 2012;74:118–33.
- [17] Vasseghi A, Khoshkalam V. Effect of outrigger panels on seismic performance of steel plate shear wall structural system. *Int J Steel Struct* 2020;20(4):1180–92.
- [18] Safari Gorji M, Cheng J-J-R. Steel plate shear walls with outriggers. Part I: Plastic analysis and behavior. *J Constr Steel Res* 2017;134:148–59.
- [19] Li C-H, Tsai K-C, Chang J-T, Lin C-H. Cyclic Test of a Coupled Steel Plate Shear Wall Substructure. *Procedia Eng* 2011;14:582–9.
- [20] Verma A, Sahoo D-R. Seismic behaviour of steel plate shear wall systems with staggered web configurations. *Earthquake Eng Struct Dyn* 2018;47(3):660–77.
- [21] Xue M, Lu L-W. Interaction of steel plate shear panels with surrounding frame members. *Proceedings of Structural Stability Research Council, Annual Technical Session, Bethlehem*. (1994) 339–354.
- [22] Choi I-R, Park H-G. Steel plate shear walls with various infill plate designs. *J Struct Eng* 2009;135(7):785–96.
- [23] Guo L, Rong Q, Ma X, Zhang S. Behavior of steel plate shear wall connected to frame beams only. *Int J Steel Struct* 2011;11(4):467–79.
- [24] Vatanserver C, Yardimci N. Experimental investigation of thin steel plate shear walls with different infill-to-boundary frame connections. *Steel Compos Struct* 2011;11(3):251–71.
- [25] Qian, X. Development of a new high-performance steel plate shear wall system with an innovative gusset plate moment connection. Ph. D. Dissertation, University of California, Berkeley, 2017.
- [26] Wei M-W, Liew J-Y-R, Xiong M-X, Fu X-Y. Hysteresis model of a novel partially connected buckling-restrained steel plate shear wall. *J Constr Steel Res* 2016;125:74–87.
- [27] Wei M-W, Liew J-Y-R, Fu X-Y. Panel action of novel partially connected buckling-restrained steel plate shear walls. *J Constr Steel Res* 2017;128:483–97.
- [28] Wei M-W, Liew J-Y-R, Du Y, Fu X-Y. Seismic behavior of novel partially connected buckling-restrained steel plate shear walls. *Soil Dyn Earthquake Eng* 2017;103:64–75.
- [29] Wei M-W, Liew J-Y-R, Du Y, Fu X-Y. Experimental and numerical investigation of novel partially connected steel plate shear walls. *J Constr Steel Res* 2017;132:1–15.
- [30] Paslar N, Farzampour A, Hatami F. Infill plate interconnection effects on the structural behavior of steel plate shear walls. *Thin-Walled Struct* 2020;149:106621.
- [31] Haji Mirsadeghi M-R, Fanaie N. Steel plate shear walls with partial length connection to vertical boundary element. *Structures* 2021;32:1820–38.
- [32] Li C-H, Tsai K-C, Lee H-C. Seismic design and testing of the bottom vertical boundary elements in steel plate shear walls. Part 2: experimental studies. *Earthquake Eng Struct Dyn* 2014;43:2155–77.
- [33] Vian D, Bruneau M, Purba R. Special Perforated Steel Plate shear walls with reduced beam section anchor beams. II: analysis and design recommendations. *J Struct Eng* 2009;135(3):221–8.
- [34] Vian D, Bruneau M, Tsai K-C, Lin Y-C. Special perforated steel plate shear walls with reduced beam section anchor beams. I: Experimental investigation. *J Struct Eng* 2009;135(3):211–20.
- [35] Choi I-R, Park H-G. Ductility and energy dissipation capacity of shear-dominated steel plate walls. *J Struct Eng* 2008;134(9):1495–507.
- [36] AISC. Seismic provisions for structural steel buildings. ANSI/AISC 341–05, American Institute of Steel Construction, Chicago, IL, 2005.
- [37] Hibbit, Karlsson and Sorensen. Abaqus standard user's manual, Inc. vols. 1, and 3. Version 6.8-1, 2008.
- [38] Driver R-G, Kulak G-L, Kennedy D-J-L, Elwi A-E. Seismic behavior of steel plate shear walls. Structural Engineering Rep. No. 215, Department of Civil Engineering, University of Alberta, Edmonton, AB, 1997.
- [39] Choi I-R, Park H-G. Hysteresis model of thin infill plate for cyclic nonlinear analysis of steel plate shear walls. *J Struct Eng* 2010;136(11):1423–34.
- [40] Qu B, Bruneau M. Behavior of vertical boundary elements in steel plate shear walls. *Eng J-Am Inst Steel Constr* 2010;47(2):109–22.
- [41] Driver R-G, Kulak G-L, Kennedy D-J-L, Elwi A-E. Cyclic tests of four-story steel plate shear wall. *J Struct Eng* 1998;124(2):112–220.
- [42] Lee C-S, Tsai K-C. Experimental Response of Four 2-Story Narrow Steel Plate Shear Walls. *Proceedings of the 2008 Structures Congress, Vancouver, BC, Canada*.
- [43] Porter D-M, Rockey K-C, Evans H-R. The collapse behavior of plate girders loaded in shear. *J Struct Eng* 1975;53(8):313–25.
- [44] Berman J, Bruneau M. Capacity design of vertical boundary elements in steel plate shear walls. *Eng J (AISC)* 2008;15.
- [45] Timler PA, Kulak GL. Experimental study of steel plate shear walls, structural engineering report No 114. Edmonton, AB: Department of Civil Engineering, University of Alberta; 1983.
- [46] CSA, Limit States Design of Steel Structures, CAN/CSA S16-94, Canadian Standards Association, Toronto, Canada, 1994.
- [47] Bruneau M, Uang C-M, Sabelli S-R. Ductile design of steel structures. McGraw-Hill; 2011.